AD-A165 968 ENVIRONMENTAL AND WATER QUALITY OPERATIONAL STUDIES 1/1
PHYSICAL MODELING OF.. (U) ARMY ENGINEER WATERWAYS
EXPERIMENT STATION VICKSBURG MS ENVIR..
UNCLASSIFIED M S DORTCH ET AL. DEC 85 WES/TR/E-85-14 F/G 13/2 NL

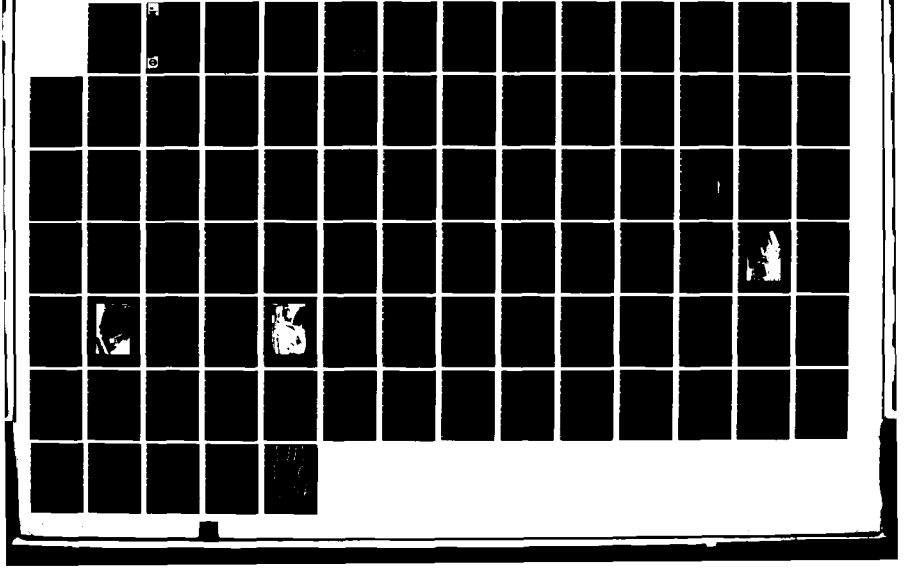

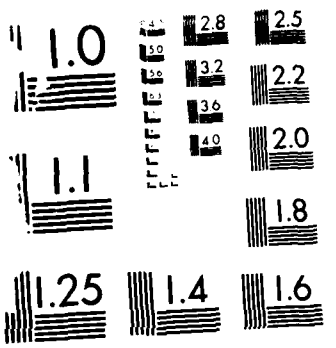

MICROCOPY RESOLUTION TEST CHART

US Army Corps of Engineers

ENVIRONMENTAL AND WATER QUALITY OPERATIONAL STUDIES

12

TECHNICAL REPORT E-85-14

PHYSICAL MODELING OF RESERVOIR HYDRODYNAMICS

by

Mark S. Dortch, Steven C. Wilhelms,
Jeffery P. Holland

Hydraulics Laboratory

DEPARTMENT OF THE ARMY
Waterways Experiment Station, Corps of Engineers
PO Box 631, Vicksburg, Mississippi 39180-0631

December 1985
Final Report

Prepared for DEPARTMENT OF THE ARMY
US Army Corps of Engineers
Washington, DC 20314-1000

Under CWIS 31593
(EWQOS Work Unit IA.3)

Monitored by Environmental Laboratory
US Army Engineer Waterways Experiment Station
PO Box 631, Vicksburg, Mississippi 39180-0631

Destroy this report when no longer needed. Do not return it to the originator.

The findings in this report are not to be construed as an official Department of the Army position unless so designated by other authorized documents.

The contents of this report are not to be used for advertising, publication, or promotional purposes. Citation of trade names does not constitute an official endorsement or approval of the use of such commercial products.

12

Unclassified

SECURITY CLASSIFICATION OF THIS PAGE (When Data Entered)

REPORT DOCUMENTATION PAGE		READ INSTRUCTIONS BEFORE COMPLETING FORM
1. REPORT NUMBER Technical Report E-85-14	2. GOVT ACCESSION NO.	3. RECIPIENT'S CATALOG NUMBER
4. TITLE (and Subtitle) PHYSICAL MODELING OF RESERVOIR HYDRODYNAMICS		5. TYPE OF REPORT & PERIOD COVERED Final report 6. PERFORMING ORG. REPORT NUMBER
7. AUTHOR(s) Mark S. Dortch Steven C. Wilhelms Jeffery P. Holland		8. CONTRACT OR GRANT NUMBER(s)
9. PERFORMING ORGANIZATION NAME AND ADDRESS US Army Engineer Waterways Experiment Station Hydraulics Laboratory PO Box 631, Vicksburg, Mississippi 39180-0631		10. PROGRAM ELEMENT, PROJECT, TASK AREA & WORK UNIT NUMBERS CWIS No. 31593 (EWQOS Work Unit IA.3)
11. CONTROLLING OFFICE NAME AND ADDRESS DEPARTMENT OF THE ARMY US Army Corps of Engineers Washington, DC 20314-1000		12. REPORT DATE December 1985 13. NUMBER OF PAGES 82
14. MONITORING AGENCY NAME & ADDRESS (if different from Controlling Office) US Army Engineer Waterways Experiment Station Environmental Laboratory PO Box 631, Vicksburg, Mississippi 39180-0631		15. SECURITY CLASS. (of this report) Unclassified 15a. DECLASSIFICATION/DOWNGRADING SCHEDULE

16. DISTRIBUTION STATEMENT (of this Report)

Approved for public release; distribution unlimited.

17. DISTRIBUTION STATEMENT (of the abstract entered in Block 20, if different from Report)

18. SUPPLEMENTARY NOTES

Available from National Technical Information Service, 5285 Port Royal Road, Springfield, Virginia 22161.

19. KEY WORDS (Continue on reverse side if necessary and identify by block number)

Density currents
Hydrodynamics
Physical modeling
Reservoirs

20. ABSTRACT (Continue on reverse side if necessary and identify by block number)

Guidance is presented for the use of physical models in the study of reservoir hydrodynamic processes. Modeling theory is developed by non-dimensionalizing the Navier-Stokes equations of fluid motion. Examination of these nondimensional equations shows that complete dynamic similitude between prototype and model is achieved by the equating of respective Froude and Reynolds numbers. Although such an equation is not possible if water is the

(Continued)

DD FORM 1 JAN 73 1473 EDITION OF 1 NOV 65 IS OBSOLETE

Unclassified

SECURITY CLASSIFICATION OF THIS PAGE (When Data Entered)

20. ABSTRACT (Continued).

model and prototype fluid, similitude is still maintained if the model and prototype Froude numbers are equated and if the fundamental character of prototype flow (turbulent) is maintained in the model.

Scaling relationships for undistorted and distorted models are presented and the appropriate use of each is discussed. Examples of the application of the relationships presented are given in some detail. An extensive list of publications documenting site-specific and research investigations involving physical modeling is also provided in the Bibliography.

PREFACE

The research reported herein was conducted during 1981 and 1982 in the Hydraulics Laboratory (HL) of the US Army Engineer Waterways Experiment Station (WES). The investigations were funded under the Environmental and Water Quality Operational Studies (EWQOS) Program, Task IA.3 "Improve and Verify Physical Hydrodynamic Modeling Techniques for Reservoir," which was sponsored by the Office, Chief of Engineers (OCE). The OCE Technical Monitors for EWQOS were Dr. John Bushman and Messrs. Earl Eiker and James L. Gottesman. The EWQOS Program was assigned to the WES under the direction of the Environmental Laboratory (EL).

Mr. Henry Simmons, Chief of the HL, and Mr. John L. Grace, Jr., Chief of the Hydraulic Structures Division (HS), directed the research. Dr. Dennis R. Smith, former Chief of the Reservoir Water Quality Branch (RWQB) in HS, supervised the effort. Messrs. Mark S. Dortch and Steven C. Wilhelms conducted the studies reported herein and prepared the bulk of this report. Assisting in laboratory work were Messrs. Calvin Buie, Alvin Myers, and James Daub. Mr. Jeffery P. Holland, Chief of the RWQB, reviewed the report and assisted in its final preparation. The report was edited by Ms. Jamie W. Leach of the WES Publications and Graphic Arts Division.

Dr. Jerome Mahloch was Program Manager of the EWQOS during these studies. Dr. John Harrison was Chief of EL. Director of WES was COL Allen F. Grum, USA. Technical Director was Dr. Robert W. Whalin.

This report should be cited as follows:

Dortch, M. S., Wilhelms, S. C., and Holland, J. P. 1985. "Physical Modeling of Reservoir Hydrodynamics," Technical Report E-85-14, US Army Engineer Waterways Experiment Station, Vicksburg, Miss.

CONTENTS

CONVERSION FACTORS, NON-SI TO SI (METRIC)
UNITS OF MEASUREMENT

Non-SI units of measurement used in this report can be converted to SI (metric) units as follows:

Multiply	By	To Obtain
cubic feet	0.02831685	cubic metres
cubic feet per second	0.02831685	cubic metres per second
Fahrenheit degrees	5/9	Celsius degrees or Kelvins*
feet	0.3048	metres
feet per second	0.3048	metres per second
gallons per minute	3.785412	cubic decimetres per minute
gallons (US liquid) per hour	3.785412	cubic decimetres per hour
inches	25.4	millimetres
square feet per second	0.09290304	square metres per second

* To obtain Celsius (C) temperature readings from Fahrenheit (F) readings, use the following formula: $C = (5/9)(F - 32)$. To obtain Kelvin (K) readings, use: $K = (5/9)(F - 32) + 273.15$.

PHYSICAL MODELING OF RESERVOIR HYDRODYNAMICS

PART I: INTRODUCTION

Background

1. In concern for environmental quality, water resource engineers and planners evaluate water quality within and released from man-made lakes or reservoirs. Typically their concerns extend over the distribution of water quality characteristics over the depth of the reservoir and the quality of water released through the reservoir flow control system. Some of the quality constituents of interest are temperature, suspended and dissolved solids, dissolved oxygen, reduced metals, and other water quality parameters. Of significant importance to the quality of water in a reservoir is the transport of these constituents into, through, and out of the reservoir.

2. A variety of techniques and tools to evaluate reservoir water quality are available to the water resource planner or engineer. Many of these tools involve transport descriptions. Physical models of varied descriptions can be used to evaluate the hydrodynamics and transport phenomena of a reservoir. Physical models are either near-field or far-field models and are used to evaluate withdrawal characteristics, inflow, entrainment, mixing, dispersion, dilution, velocity patterns, and density currents. One-dimensional numerical water quality models are used extensively to evaluate the thermal and quality regimes of a reservoir. Two-dimensional numerical models are being developed for evaluating hydrodynamics and thermal and quality aspects of a reservoir along two axes (usually the vertical and longitudinal axes) simultaneously. Hybrid modeling, which entails a combination of physical and numerical modeling, can be used to provide higher quality evaluations of the reservoir environment.

3. Near-field physical models reproduce localized hydrodynamics. Local mixing, entrainment, and withdrawal flow conditions can be simulated and their characteristics can be defined. For hybrid modeling,

mixing, entrainment, or withdrawal is physically simulated, mathematically quantified, and incorporated into numerical models. The near-field physical model provides a site-specific description of the localized hydrodynamics that result in a more accurate description of boundary conditions in the numerical model.

4. Far-field physical models simulate the overall water body hydrodynamics extending beyond the localized flow field typically investigated in a near-field model. The effects of complex geomorphology or operations have been investigated in far-field models. Of interest in these models are the effects of local mixing upon the far-field and the velocity patterns and movement of density currents through the reservoir. The results from these models are usually incorporated into a numerical model, exemplifying the hybrid modeling approach.

5. Physical and numerical models typically complement each other. The information gained with one model is enhanced by the knowledge gained from the other. However, neither numerical nor physical models can be used indiscriminately. Numerical models are no more accurate than the assumptions associated with their development and the numerical procedure used to arrive at a solution. Physical models are no more accurate than their scaling criteria. Some physical aspects of prototypes are exaggerated in a model; for instance, bottom roughness may be disproportionately large in a physical model. This does not preclude the use of physical models. Rather, these models yield excellent results if geometric and hydrodynamic similarity is preserved. Additionally, for complex boundary or operational conditions, physical models may be the only practical technique to describe the hydrodynamics.

Purpose and Scope

6. The objective of this report is to overview the applicability of scaled physical models for the solution of water resources problems. Particular attention will be given to the evaluation/verification of the criteria used to scale various reservoir hydrodynamic processes in physical models. These processes include selective withdrawal, density

currents, hydraulic jets, and mixing processes. Undistorted and distorted physical model scaling relationships are presented with emphasis on criteria for model distortion. Example applications of physical models are presented and distorted model-prototype comparisons are made. The theoretical basis of general scaling relationships for physical models, although well established and documented in other texts, is also presented in order to provide the reader access to these concepts within a single document.

PART II: FROUDIAN SCALING FOR PHYSICAL MODELS

Modeling Theory

7. Dimensionless groupings that characterize stratified flow can be deduced from the Navier-Stokes equations. From these groupings, scaling criteria can be developed for use in the application of physical modeling to water resource problems. If incompressibility is assumed, these equations may be expressed in vector notation as

$$\frac{\partial \bar{q}}{\partial t} + \bar{q} \cdot \nabla \bar{q} = \bar{g} - \frac{1}{\rho} \nabla p + \frac{\mu}{\rho} \nabla^2 \bar{q} \qquad (1)$$

where

$\bar{q} = u\bar{i} + v\bar{j} + w\bar{k}$, a three-dimensional velocity vector

u,v,w = velocity in the x-, y-, z-direction, respectively

t = time

$\bar{q} \cdot \nabla$ = "dot" product of the velocity vector and ∇

∇ = gradient operator, $\frac{\partial}{\partial x} \bar{i} + \frac{\partial}{\partial y} \bar{j} + \frac{\partial}{\partial z} \bar{k}$

$\bar{g}$ = gravitational acceleration vector

ρ,μ = fluid density and viscosity, respectively

p = pressure

∇^2 = Laplacian operator, $\frac{\partial^2}{\partial x^2} + \frac{\partial^2}{\partial y^2} + \frac{\partial^2}{\partial x} 2$

8. Introducing a small density perturbation ρ' such that $\rho = \rho_o + \rho'$ (where ρ_o is the density of a homogeneous fluid and $(\rho'/\rho_o) << 1$) will result in approximating incompressibility and will allow the effects of density differences to appear in the equation. Let the pressure term p be defined such that

$$p = p_c + \rho_o \bar{g} \cdot \bar{r} + p' \qquad (2)$$

where

p_c = known pressure at reference location c

$\bar{r}$ = vector from location c to location of p

p' = pressure perturbation from homogeneous, hydrostatic fluid

Substituting for p, Equation 1 becomes

$$\frac{\partial \bar{q}}{\partial t} + \bar{q} \cdot \nabla \bar{q} = \bar{g} - \frac{1}{\rho_o + \rho'} \nabla (p_c + \rho_o \bar{g} \cdot \bar{r} + p') + \frac{\mu}{\rho_o + \rho'} \nabla^2 \bar{q} \qquad (3)$$

The coefficient of the pressure term may be expanded in a binomial series,

$$\frac{1}{\rho_o + \rho'} = \frac{1}{\rho_o} \left(1 + \frac{\rho'}{\rho_o}\right)^{-1} = \frac{1}{\rho_o} \left[1 - \frac{\rho'}{\rho_o} + \left(\frac{\rho'}{\rho_o}\right)^2 - \ldots\right] \qquad (4)$$

Assuming that the second-order and higher order terms in Equation 4 are approximately zero (which is reasonable since $(\rho'/\rho_o) << 1$) and since $\nabla p_c = 0$ (p_c by definition is constant), $\nabla \bar{g} \cdot \bar{r} = \bar{g}$, and $(\rho'/\rho_o)^2 \nabla p' \simeq 0$ (ρ' and p' are small), the pressure term (Equation 2) may be reduced to

$$\bar{g} + \frac{1}{\rho_o} \nabla p' - \frac{\rho' \bar{g}}{\rho_o} \qquad (5)$$

Letting $\rho' = \Delta\rho$, some small incremental density difference, and $\mu/(\rho_o + \rho') = \nu$, kinematic viscosity, and substituting Equation 5 into the pressure term of Equation 3, the equation of fluid motion based on the Boussinesq incompressibility approximation can be written as

$$\frac{\partial \bar{q}}{\partial t} + \bar{q} \cdot \nabla \bar{q} = \frac{\Delta\rho}{\rho_o} \bar{g} - \frac{1}{\rho_o} \nabla p' + \nu \nabla^2 \bar{q} \qquad (6)$$

9. To develop similitude criteria for modeling, Equation 6 should be nondimensionalized. By orienting the z-axis in the vertical direction (measured positive upward) the components of the gravitational vector $\bar{g}$ become

$$\bar{g} = -g\bar{k}$$

where $\bar{k}$ is the unit vector in the z-direction. The z-component of Equation 6 is

$$\frac{\partial w}{\partial t} + \frac{u\partial w}{\partial x} + \frac{v\partial w}{\partial y} + \frac{w\partial w}{\partial z} = -\frac{\Delta\rho}{\rho_o} g - \frac{1}{\rho_o}\frac{\partial p'}{\partial z} + \nu\left(\frac{\partial^2 w}{\partial x^2} + \frac{\partial^2 w}{\partial y^2} + \frac{\partial^2 w}{\partial z^2}\right) \qquad (7)$$

Equation 7 can be made nondimensional with the following relationships:

$$\hat{w} = \frac{w}{U}\ ,\ \hat{t} = \frac{t}{L/U}\ ,\ \hat{u} = \frac{u}{U}\ ,\ \hat{v} = \frac{v}{U}$$

$$\hat{x} = \frac{x}{L}\ ,\ \hat{y} = \frac{y}{L}\ ,\ \hat{z} = \frac{z}{L}$$

$$\hat{p}' = \frac{p'}{\rho_o U^2}$$

where the "^" denotes a dimensionless variable, ρ_o , ν, g are constants, and

U = characteristic velocity

L = characteristic length

Substituting the above expressions into Equation 7 and simplifying the result in an equation that, when multiplied by L/U^2, is a dimensionless mathematical description of fluid motion in the z-direction:

$$\underbrace{\frac{\partial \hat{w}}{\partial \hat{t}} + \hat{u}\frac{\partial \hat{w}}{\partial \hat{x}} + \hat{v}\frac{\partial \hat{w}}{\partial \hat{y}} + \hat{w}\frac{\partial \hat{w}}{\partial \hat{z}}}_{\text{Inertial Force}} = \underbrace{-\frac{\Delta\rho}{\rho_o} g \frac{L}{U^2}}_{\substack{\text{Gravita-}\\ \text{tional}\\ \text{force}}} \underbrace{-\frac{\partial \hat{p}'}{\partial \hat{z}}}_{\substack{\text{Pres-}\\ \text{sure}\\ \text{force}}} + \underbrace{\frac{\nu}{UL}\left(\frac{\partial^2 \hat{w}}{\partial \hat{x}^2} + \frac{\partial^2 \hat{w}}{\partial \hat{y}^2} + \frac{\partial^2 \hat{w}}{\partial \hat{z}^2}\right)}_{\substack{\text{Viscous}\\ \text{Force}}} \qquad (8)$$

A similar equation may be written for the x- and y-directions. This equation contains two dimensionless parameters that are familiar to hydraulicians and hydrodynamicists: the Reynolds number (Re), which is the inverse of the coefficient in the viscous force term; and the densimetric Froude number (Fr; hereafter referred to as the Froude number), which is the inverse square root of the coefficient in the gravitational force term.

10. For dynamic similitude, the ratios of prototype forces to homologous model forces must be equal. That is, from Equation 8, the ratio of prototype inertial forces to model inertial forces must equal

the ratio of prototype-to-model gravitational forces, which must equal the ratio of prototype-to-model viscous forces, which must equal the ratio of prototype-to-model pressure forces. Examination of Equation 8 shows that the equating of the respective prototype and model Froude and Reynolds numbers results in the ratios of the gravitational and viscous prototype-to-model forces being equal to unity. Since the equation is dimensionless, this further dictates that the ratio of the respective inertial forces be unity as well. From the previous definition of dynamic similitude, the ratio of prototype-to-model pressure forces must also be unity. Thus, the equating of respective prototype and model Froude and Reynolds numbers ensures the existence of complete dynamic similitude.

11. It is usually impossible to provide complete dynamic similitude since scale reductions affect some dimensionless ratios. However, one or more of the forces may be absent or negligible for a given flow regime. In fluid systems with a free surface, such as open hydraulic channels, and water bodies, such as reservoirs, inertial, pressure, and gravitational forces often dominate. Thus, the Froude number should be preserved when scaling from prototype to model.

12. However, although gravitational forces are of major importance when modeling open channel hydraulics, viscous and surface tension forces are not always negligible. For reservoirs and other large water bodies, viscous forces may be important in some flow regimes. Since water is used in most models of hydraulic systems, it is not possible to simultaneously preserve Froude and Reynolds number equalities. Experience has shown that if the fundamental character of flow is preserved in both prototype and model (i.e., both systems are turbulent), then similitude relationships, valid for transfer of quantities from model to prototype, can be developed based on the Froude number only for open channel hydraulics. Limitations and requirements for Froudian modeling when viscous forces are important are discussed in Part III.

Scaling Relationships

13. The Froudian scaling criterion for density stratified flow

dictates that the Froude number be equal in model and prototype. That is

$$Fr_m = Fr_p$$

or

$$\frac{V_m}{\sqrt{\frac{\Delta\rho_m}{\rho_m} gL_m}} = \frac{V_p}{\sqrt{\frac{\Delta\rho_p}{\rho_p} gL_p}} \tag{9}$$

where

m,p = model and prototype, respectively

V_m, V_p = velocity in model and prototype, respectively

$\Delta\rho_m$, $\Delta\rho_p$ = density difference, model and prototype, respectively

ρ_m, ρ_p = density in model and prototype, respectively

g = gravitational acceleration

L_m, L_p = characteristic length in model and prototype, respectively

By providing identical density differences in model and prototype such that

$$\frac{\Delta\rho_m}{\rho_m} = \frac{\Delta\rho_p}{\rho_p}$$

the Froudian scaling relations for velocity, time, and discharge can be simplified. This relationship is assumed in subsequent modeling criteria.

14. Undistorted near-field reservoir models have equal horizontal and vertical scales. These models are geometrically and hydrodynamically similar to the prototype. Distorted scale reservoir models typically have a vertical scale that is exaggerated with respect to the horizontal scale to allow sufficient depth to produce turbulent flow and permit stratified flow visualization. This results in different scaling relationships for undistorted and distorted models.

Undistorted modeling

15. Several scaling relationships are required for the design of an undistorted model. These include length, velocity, time, and discharge. The velocity scale relation is determined by rearranging Equation 9 into a velocity ratio (denoted by the upper case R subscript) for model and prototype.

$$V_R = \frac{V_p}{V_m} = \frac{\sqrt{\frac{\Delta\rho_p}{\rho_p} gL_p}}{\sqrt{\frac{\Delta\rho_m}{\rho_m} gL_m}} \tag{10a}$$

Cancelling terms results in

$$V_R = \sqrt{\frac{L_p}{L_m}} = L_R^{1/2} \tag{10b}$$

The velocity scaling ratio is the square root of the length ratio. The time scale relationship is determined by substituting velocity L/t for V in Equation 9. Cancelling terms again results in a time scale ratio

$$t_R = \frac{t_p}{t_m} = \sqrt{\frac{L_p}{L_m}} = L_R^{1/2} \tag{11}$$

where t_m, t_p = time in the model and prototype, respectively. To determine the discharge scaling function, the continuity relationship is used:

$$Q = AV$$

where

Q = volumetric flow rate

A = cross-sectional area of flow

V = velocity of flow

Solving for velocity from the continuity equation and substituting into Equation 9 results in the discharge scaling relationship:

$$Q_R = \frac{Q_p}{Q_m} = \frac{L_p^2}{L_m^2}\sqrt{\frac{L_p}{L_m}} = L_R^{5/2} \tag{12}$$

Distorted modeling

16. Scale relations for distorted scale physical models can be developed in an analogous manner with slight differences. The horizontal and vertical length scale ratios for a distorted model are defined as

$$X_R = X_p/X_m \tag{13a}$$

and

$$Y_R = Y_p/Y_m \tag{13b}$$

where

X_R, Y_R = length scale ratios in horizontal and vertical directions, respectively

X_p, Y_p = prototype length in horizontal and vertical directions, respectively

X_m, Y_m = length of model in horizontal and vertical directions, respectively

In a distorted model, the scaling ratio for area in a horizontal plane A_{x_R} is

$$A_{x_R} = X_R^2 \tag{14a}$$

while in a vertical plane the area scaling ratio is

$$A_{y_R} = X_R Y_R \tag{14b}$$

The characteristic length in the gravitational term (denominator) of Equation 9 is in the y-direction, the direction of gravity. Therefore,

velocity scaling for a distorted model uses model length in the vertical direction Y_R. Substituting Y_R into Equation 9 and solving for the velocity ratio yields

$$V_R = \frac{V_p}{V_m} = \left(\frac{Y_p}{Y_m}\right)^{1/2} = Y_R^{1/2} \tag{15}$$

For the time scale, letting $V = L/t$ and defining the characteristic length to be in the x-direction, yields

$$t_R = \frac{t_p}{t_m} = X_R/(Y_R)^{1/2} \tag{16}$$

Using the continuity relationship $Q = AV$ and Equation 15, the discharge relationship is

$$Q_R = \frac{Q_p}{Q_m} = \frac{A_p}{A_m}(Y_R)^{1/2} \tag{17}$$

where A_m and A_p = flow area in model and prototype, respectively. The area of flow is a vertical cross section; therefore, flow area is defined for the model and prototype, respectively, as

$$A_m = A_{y_m} = X_m Y_m \tag{18a}$$

and

$$A_p = A_{y_p} = X_p Y_p \tag{18b}$$

where the lower case y subscript denotes the vertical cross-sectional area. Substituting Equations 18a and 18b into Equation 17 results in the following discharge ratio for distorted scales

$$Q_R = X_R Y_R^{3/2} \tag{19}$$

17. The scaling relationships are summarized in the following tabulations:

Dimension	Ratio
Undistorted Model	
Length	$L_R = L_p/L_m$
Velocity	$V_R = L_R^{1/2}$
Time	$t_R = L_R^{1/2}$
Volume flow rate	$Q_R = L_R^{5/2}$
Density difference	$\Delta\rho_R = 1$
Distorted Model	
Length in the horizontal	$X_R = X_p/X_m$
Length in the vertical	$Y_R = Y_p/Y_m$
Area in the horizontal plane	$A_{x_R} = X_R^2$
Area in the vertical plane	$A_{y_R} = X_R Y_R$
Velocity	$V_R = Y_R^{1/2}$
Time	$t_R = X_R/Y_R^{1/2}$
Volume flow rate	$Q_R = X_R Y_R^{3/2}$
Density difference	$\Delta\rho_R = 1$

18. Model-to-prototype length scale ratios for an undistorted model may range from 1:5 to 1:200, depending on the area and flow regime of interest. Distorted scales may range from 1:800 to 1:4,000 in the horizontal (X_R) and 1:20 to 1:200 (Y_R) in the vertical. Typically, distortion factors X_R/Y_R may range from 4 to 40.

PART III: DISCUSSION OF THE ROLE OF DISTORTION IN RESERVOIR MODELING

Criteria for Distortion

19. When modeling a large open water body such as a surface reservoir, there may be several flow regimes of interest such as those dominated by inertia, buoyancy, and turbulent dispersion. One may be interested in not only what occurs near a perturbation, but also what occurs at some distance (far field). Modeling for several interests simultaneously may require conflicting modeling criteria. Froudian laws are still required to give the proper balance between inertial and gravitational forces, but vertical length scale exaggeration or distortion may be necessary to provide adequate turbulence and proper viscous effects.

20. Modeling such large water bodies often necessitates for economy of size a large horizontal length scale ratio X_R where

$$X_R = \frac{X_p}{X_m}$$

and X_p and X_m are the horizontal dimensions of the prototype and model, respectively. With a large horizontal scale ratio, a smaller vertical scale ratio Y_R must usually be selected to provide adequate model depth for data collection and turbulent flow. Thus, the vertical scale is exaggerated or distorted and the distortion factor DF is

$$DF = \frac{X_R}{Y_R}$$

The concerns related to this modeling are how much distortion is needed and what is too much. The answers to these questions depend on the physical processes under study and an understanding of the modeling features that may be lost or compromised for a given factor of distortion.

21. Physical processes that may be of interest in a reservoir model include inflow, outflow, density currents, turbulent mixing and

dispersion, buoyant jets, and heat exchange. These processes are affected by the geometry, densimetric Froude number, Reynolds number, bottom roughness, and coefficient of surface heat exchange. A discussion of the modeling of these processes is presented in the context of distorted reservoir model applicability based on equality of the densimetric Froude number and density differences and approximately equal density and viscosity (same fluid, water) in the prototype and model ($\rho_R = \Delta\rho_R = \mu_R = 1.0$ for the prototype/model ratios of density, density difference, and viscosity, respectively).

Inflow and outflow

22. Inflow and outflow are boundary conditions for the resulting internal currents in density stratified reservoirs. The volumetric flow rates for inflow and outflow are scaled according to Froudian scaling as presented in paragraph 16. This scaling is appropriate for inflow since inertia and buoyancy will be properly accounted for in the model.

23. In some instances, simply using distorted Froudian scaling criteria may not result in simulating the vertical extent of the zone of withdrawal during outflow. Many reservoir outlets can be well described as point sinks (Bohan and Grace 1973). The vertical distance from the elevation of the sink to the upper or lower withdrawal limit Z is dependent upon the discharge Q and the density difference between the elevations of the sink and the withdrawal limit $\Delta\rho$ This distance can be approximated by

$$Z \propto \left(\frac{Q}{\sqrt{\frac{\Delta\rho}{\rho} g}} \right)^{2/5} \tag{20}$$

The limits of withdrawal should scale according to the vertical length scale such that $Z_R = Y_R$ where Z_R equals the ratio of prototype limit to model limit. Substituting $Q_R = X_R Y_R^{3/2}$ (Froudian discharge scaling from Equation 19) and $\rho_R = \Delta\rho_R = 1.0$ into the above equation, it is obvious that Z_R will not equal Y_R but $(DF)^{2/5} Y_R$. Therefore, for the general case of a long reservoir (DF > 1), the model withdrawal zone would not extend as far vertically as the prototype withdrawal zone. If

the outlet is a rectangular orifice, then direct horizontal and vertical scaling results in a vertical model dimension stretched with respect to the horizontal dimension. This allows some remedy to the dilemma since such stretched outlets may cause a deepening of the withdrawal zone beyond that described for a point sink. To simulate point sink withdrawal, it may be necessary to adjust the vertical extent of the outlet opening to simulate the withdrawal limits for the specified scaled discharge.

24. When a prototype release structure can be catagorized as discharge through a line sink, adjustments to the model outlet should not be necessary. This is because

$$Z \propto \left(\frac{q}{\sqrt{\frac{\Delta\rho}{\rho} g}} \right)^{2/3} \tag{21}$$

where q is the unit discharge. Using the discharge scaling stated in paragraph 23, it is apparent that the above equation results in $Z_R = Y_R$. It should be emphasized that distorted reservoir models are not intended for comprehensive analysis of the near-field withdrawal distribution. This type of analysis is usually conducted with an undistorted model with a length scale ratio L_R equal to both X_R and Y_R.

Density currents

25. Even if the inflow-outflow boundary conditions have been properly established, the resulting model density currents (convective spreading) must be evaluated for similitude. The interfacial shear stress developed by a layer of fluid flowing above or beneath another layer of fluid may be disproportionately large in an undistorted model compared with inertial and gravitational forces. The bottom shear may also be disproportionately large in an undistorted model if the model roughness is too great. Vertical scale exaggeration in a distorted model is often used to compensate for excess shear and bottom roughness.

26. Proper adjustment for bottom roughness is required when attempting to model density currents flowing along the bottom (underflows) and to provide similar damping of internal waves. In an undistorted

model, the scaling ratio for the Manning's n roughness factor is

$$n_R = L_R^{1/6} \tag{22}$$

If the prototype bottom is fairly smooth, as with a sandy bottom, it may be impossible to decrease the model n sufficiently since the model boundary may already be hydrodynamically smooth. However, this may be overcome through vertical scale exaggeration where the scale relation for n is

$$n_R = \frac{Y_R^{1/6}}{\sqrt{DF}} \tag{23}$$

Thus, it may be possible to provide the proper roughness effect by using a smooth model boundary and adjusting the distortion factor. Usually it is desirable to have $DF > Y_R^{1/3}$; therefore, n_m must be greater than n_p . This, in turn, requires exaggerated roughness elements and calibration procedures for proper physical model adjustment.

27. When the bottom is relatively flat, bottom roughness adjustment alone may be sufficient for modeling bottom density currents. When modeling river or channel flow, it may be necessary to adjust the bed slope and roughness in a distorted-length scale model to give the proper stage-discharge relationship. With a reservoir model, the water surface is flat and the depth may vary considerably from the headwater to the dam. If the model is to reproduce the capacity-elevation characteristics of the prototype, then it would not be possible to reduce the bed slope to account for the excessive steepness caused by distortion. In some instances this may necessitate an adjustment to the bed roughness to compensate for the excessive slope.

28. Interflow and overflow (surface flow) density currents are affected by interfacial shear. A discussion of interflow and overflow phenomena can be found in Appendix A. Because nonviscous intrusion (interflow and overflow) characteristics are dependent on Froude number, Froudian scaling (distorted or undistorted) should properly simulate a

nonviscous prototype intrusion if the intrusion in the model is also in the nonviscous range. However, length scale distortion may be required to ensure that a nonviscous intrusion will exist in the model. To illustrate this, it is first assumed that the density, density difference, and viscosity of the model equal that of the prototype. Then, if the criteria from Appendix A for nonviscous spreading are maintained in the model when there is nonviscous spreading in the prototype, from Equation A9

$$\frac{\ell_R}{h_{K_R}^{5/2}} \geq 1.0 \tag{24}$$

where

ℓ_R = the ratio of prototype inflow intrusion length to analogous model length

h_{K_R} = the ratio of total prototype inflow thickness to analogous model thickness

which is the required relationship to maintain properly scaled viscous forces. An undistorted model would require $L_R \leq 1.0$ to satisfy the above relation, which means the model would have to be at least as large as the prototype. A distorted model would require

$$Y_R \leq (DF)^{2/3}$$

The distorted-scale requirements are not as restrictive as the undistorted, although Y_R may still be prohibitive. Rearranging the above relationship, the minimum distortion required to provide complete similitude for convective spreading is dependent on the vertical or horizontal scale selected, such that

$$DF \geq Y_R^{1.5} \tag{25a}$$

or

$$DF \geq X_R^{0.6} \tag{25b}$$

29. Providing nonviscous spreading in the model for the complete range of nonviscous spreading in the prototype may require fairly large distortion factors. For example, if a horizontal length scale ratio of 1,000 is selected, Equation 25b calls for $DF \geq 63$ which results in $Y_R = 15.85$. This amount of distortion and the resulting Y_R may be undesirable and unnecessary. A larger vertical length scale ratio Y_R may be more practical from a model construction and operation perspective. Additionally, if too much distortion is used, wall and end effects may be introduced. Further, excessive distortion can result in excessive horizontal (longitudinal and lateral) dispersion (which will be discussed later). To avoid such problems, a distortion factor less than that specified by Equation 25b is accepted, often without compromising similitude for the nonviscous density currents of interest. For example, the nonviscous spreading zone may extend beyond the area of interest. The distortion should be sufficiently large to ensure that the prototype nonviscous spreading distance of interest ℓ_p remains nonviscous for the scaled distance ℓ_m in the model. Existence of the nonviscous condition can be estimated for the prototype and model for interflow and overflow conditions. However, a viscous intrusion slows down and becomes thicker with time as buoyant and viscous forces dominate. Froudian modeling criteria would therefore no longer be applicable for similitude. Thus, similitude for a Froudian model may lapse when viscous convective spreading occurs. These points are discussed in greater detail in Appendix A.

Far-field dispersion

30. As indicated earlier, Froudian scaling will not preserve the prototype-model Reynolds number. The undistorted model Reynolds number will be less than the prototype. However, for many near-field flow problems, the flow is very turbulent and the area of interest is of short length (such as a hydraulic jump). For these cases, the dissipation of energy is mostly due to turbulent fluctuations rather than laminar viscous effects. Turbulent fluctuations are proportional to the square of the average velocity, as are the inertial forces; thus, dissipative forces associated with short, very turbulent flows are similar in

undistorted Froudian models. Therefore, near-field turbulent diffusion, which is also related to turbulent fluctuations, can be simulated with undistorted Froudian models. For far-field dispersion problems, the flow patterns most likely will not be short and not as turbulent as near-field problems. This makes it more difficult to account for dissipative forces and turbulent fluxes. Viscous forces and laminar diffusion in the model may dominate the turbulent fluctuations. With an undistorted far-field model, a reasonable length scale would most likely result in such a shallow depth that turbulent flow may not occur in the model. Thus, the vertical scale is exaggerated and a distorted model is used to attain turbulent flow. From Froudian law with length scale distortion, the required scale ratios for proper horizontal (transverse) and vertical dispersion are

$$D_{x_R} = \frac{X_R^2}{t_R} = X_R\, Y_R^{1/2} = DF\, Y_R^{1.5} \tag{26a}$$

$$D_{y_R} = \frac{Y_R^2}{t_R} = \frac{Y_R^{2.5}}{X_R} = \frac{Y_R^{1.5}}{DF} \tag{26b}$$

31. The actual transverse dispersion coefficient Dx for an open channel is proportional to the product of the shear velocity u^* and the depth d. For a wide channel

$$D_x \propto du_* = d\sqrt{gds_e} \tag{27}$$

where s_e is the energy slope. Therefore, the prototype-to-model ratio for transverse dispersion using Equation 27 is

$$D_{x_R} \propto \frac{Y_R^{1.5}}{\sqrt{DF}} \tag{28}$$

Thus it is apparent that the transverse model dispersion may not be scaled appropriately by Equation 28. Consider that density stratification and turbulence affect the vertical dispersion. These effects have been represented as

$$D_y = D_{y_o} f(R_i) \tag{29}$$

where

D_{y_o} = diffusion coefficient related to velocity and depth in a nonstratified reservoir

$f(R_i)$ = a function of Richardson number R_i

Froudian scaling criteria preserve the prototype/model R_i (R_i is approximately equal to the inverse of the Froude number squared). In general, $D_{y_o} \propto ud$, where u is horizontal velocity. Thus the vertical scale ratio for dispersion takes the form

$$D_{y_R} \propto Y_R^{1.5} \tag{30}$$

Again model dispersion scales differently from that desired (Equation 26b).

32. In the distorted model, dispersion can be physically related to the scale ratios by Equations 28 and 30. The desired scale relations for dispersion in the distorted model are defined by Equations 26a and 26b. The desired and actual distorted scale relationships for dispersion are summarized below:

Direction	Desired Distorted Scale Ratio for Dispersion	Actual Distorted Scale Ratio for Dispersion
Horizontal (Transverse)	$D_{x_R} = DF\ Y_R^{1.5}$	$D_{x_R} \propto \frac{Y_R^{1.5}}{\sqrt{DF}}$
Vertical	$D_{y_R} = \frac{Y_R^{1.5}}{DF}$	$D_{y_R} \propto Y_R^{1.5}$

From examination of the above relationships, it is evident that turbulent dispersion in the distorted model is too fast (overpredicted) in the horizontal (transverse) directions and too slow (underpredicted) in the vertical direction. Evidence of this result was reported by Crickmore (1972) (as referenced on p 304 in Mixing in Inland and Coastal Waters; Fischer et al. 1979) with a comparison of model and prototype observations of dispersion of a continuous source tracer. The model plume spread faster horizontally and slower vertically than the prototype plume. Similar results for lateral dispersion were found by Moretti and McLaughlin (1974) during laboratory reservoir inflow experiments designed to determine the effects of distortion. With careful adjustment of model roughness (flow inhibitors), it is possible to alter transverse and vertical mixing to improve far-field dispersion modeling. Despite possible inaccuracies in dispersion modeling, distortion is required when modeling large water bodies in order to preserve turbulent flow and to reduce shear stresses for nonviscous spreading of density currents.

Buoyant jets/plumes

33. Source momentum, buoyancy, and geometry are all important when modeling the characteristics of a free turbulent shear flow jet/plume (here simply jet unless otherwise noted). The turbulent shear flow causes the entrainment of ambient fluid, thereby increasing the volume flux of the jet along its trajectory. If an undistorted model jet is sufficiently turbulent, similitude can be preserved through Froudian scale relationships (see paragraph 30). However, a distorted model alters the model source geometry from that of the prototype. This alteration may change other jet characteristics such as entrainment. Thus, jet modeling should be accomplished without distortion in a near-field model. How can the proper effects of an undistorted jet model be created in a distorted scale model?

34. If a line diffuser (line source) is being modeled, then methods outlined in Chapter 10 of Mixing in Inland and Coastal Waters (Fischer et al. 1979) can be used to size the diffuser in the distorted model. The diffuser port sizes and spacing are kept undistorted by scaling according to the vertical scale, and the number of model ports is

reduced by the distortion factor. Scaling procedures are not as simple when a point or single source diffuser and jet is being modeled. The jet entrainment, dilution, and volume flux characteristics must be known (possibly from results of a near-field undistorted model), and the distorted model source geometry must be adjusted to yield the same characteristics in the distorted model. If the jet behavior can be estimated from relationships developed from previous analytical and experimental general investigations, then it may be possible to design a distorted model jet that will give similar behavior. An example of such a procedure is presented in Appendix B.

Heat exchange

35. Reservoir and lake water temperatures are primarily driven by hydrological and meteorological conditions and display seasonal variations (unless the lake is used for cooling thermal discharges). It would be impractical, if not impossible, to model heat exchange characteristics over a season in a physical model. If the model simulation time is not too long (several weeks), meteorological effects (such as solar heating) can be neglected, and the model can be used to analyze the reservoir hydrodynamics for the event of interest.

36. Modeling receiving waters for thermal discharges (as from a power plant) may require modeling surface heat exchange if the receiving water of interest covers a very large area. Modeling surface heat exchange requires

$$k_R = \left(\frac{K}{\gamma c_p u}\right)_R = 1.0 \qquad (31)$$

where

k_R = surface heat exchange coefficient ratio

K = surface heat exchange coefficient, Btu/ft^2/°F/sec

γ = specific weight of water, lb/ft^3

c_p = specific heat of water, Btu/lb/°F

u = characteristic velocity, ft/sec

With $(\gamma c_p)_R = 1.0$, similitude requires $K_R = \sqrt{L_R}$. Thus, K_m should be less than K_p by the ratio $\sqrt{L_R}$. This can be achieved by

controlling the atmosphere in the laboratory. If the laboratory does not have atmospheric control, it may be necessary to use distortion to compensate for the excessive heat loss rate in the model. Methods for determining the amount of distortion needed are discussed in Chapter 10 of Mixing in Inland and Coastal Waters (Fischer et al. 1979).

Model-Prototype Comparison

37. Tests were conducted at WES to compare prototype and distorted model behavior. Two lake hydrodynamic processes were studied. First, interflow and overflow (surface flow) density currents were examined with "prototypes" and models. Then, hydraulic (water jet) destratification was tested for "prototype" and model conditions.

Density currents

38. Two studies were conducted to compare distorted model versus "prototype" density current observations. One model comparison was for DeGray Lake, which is a Corps lake in Arkansas. The other comparison was for a distorted model of the 80.0-ft-long* general reservoir flume (referred to as the General Reservoir Hydrodynamic (GRH) Facility) located in the Hydraulics Laboratory of WES. In this case, the GRH was the "prototype."

39. DeGray Lake model study. Flood events on the Caddo River were simulated in a distorted scale physical model of DeGray Lake. The flood events had been observed (Ford, Johnson, and Monusmith 1980) and tracked in the prototype. Model and prototype observations were compared to identify similarities and disparities and areas of modeling theory, techniques, and procedures that should be improved.

40. The model had a horizontal scale ratio of 2,400 and a vertical scale ratio of 120, with a distortion factor of 20. Based on Froudian scaling criteria (distorted model scaling relationships in paragraph 17) the following scale ratios may be used to quantitatively transfer model data to prototype equivalents:

---

* A table of factors for converting non-SI units of measurment to SI (metric) is presented on page 3.

Dimension	Scale
Length in the horizontal	2,400
Length in the vertical	120
Area in the horizontal	5,760,000
Area in the vertical	288,000
Velocity	10.9545
Time	219.089
Volume flow rate	3,154,881.934
Density	1

The model was constructed of clear plastic to permit flow visualization. The elevation-storage relationship and general lake geometry were reproduced. No attempt was made to simulate roughness of the lake bottom or sides.

41. Three flood events were studied in the model: 29 March 1979, 14 November 1978, and 24 October 1976. Plate 1 shows the density structure of the lake for each of the three events. The density profiles were based on the thermal structure of the lake at the time of each flood event. These observed density differences between the lake epilimnion and hypolimnion and epilimnion and inflow were simulated with fresh and saline waters. Plate 1 also shows the stratification patterns used in the physical simulations. As indicated in Plate 1, the model stratification, although not exact replicates, did approximate prototype stratification. Recreating density differences is relatively easy, but reproducing the exact prototype density distribution in the model is much more difficult. Plates 2-4 show the flood hydrographs. The hydrographs were reproduced by controlling inflow with a manually operated valve. The movement of the inflow was tracked in the model by dying the inflow and marking the leading edge at specific times during each test. The inflow movement was tracked in the prototype (Ford, Johnson, and Monusmith 1980) by mapping the movement of inflow turbidity, temperature, and other naturally occurring tracers of fluorescent dye that was

injected into the river upstream of the lake.

42. Model-to-prototype comparisons were made by comparing travel time and distance measured along the mainstem of the Caddo River. To ensure a realistic comparison of model and prototype travel times, time zero was selected to be the earliest prototype data point location. Subsequent prototype observations were referenced to this time zero. Similarly, model data (after conversion to prototype equivalents) were also referenced to this time-zero location. This negated any model-prototype differences in inflow timing.

43. Figure 1 shows results of tests of the 29 March 1979 flood event. The model reproduced the movement of the density current for this event very well. Equation A6 was evaluated with the following prototype data: $h_T \simeq 33$ ft , $\Delta\rho_T \simeq 0.00105$ g/cc , $\rho = 1.0000$ g/cc , $\nu = 10^{-5}$ ft^2/sec , and $\ell \simeq 24{,}300$ ft . This yielded a value of 473 which indicated that the prototype is in the nonviscous flow regime (see Appendix A). Model data of $h_T \simeq 0.3$ ft , $\Delta\rho_T = 0.00085$ g/cc , $\rho = 1.0000$ g/cc , $\nu = 10^{-5}$ ft^2/sec , and $\ell \simeq 8.3$ ft yielded a value of about 98, indicating that model flow is also in the nonviscous flow regime. Since the model and prototype were in the nonviscous flow regime, the model reproduced the movement of the prototype current very well. This should be expected since it was entirely consistent with the theory presented in Appendix A.

44. For two of the flood events that were simulated, 14 November 1978 and 24 October 1976, the nose of the density currents moved slower in the model than in the prototype throughout most of the tests (Figures 2 and 3). This is probably due to the existence of a viscous flow regime. Typically, intrusion speed tends to decrease as viscous forces start dominating current movement. Using observed data from the 14 November 1978 event: $h_T = 8.5$ ft , $\Delta\rho_T = 0.00072$ g/cc , $\rho = 1.0$ g/cc , $\nu = 10^{-5}$ ft^2/sec , and $\ell = 26{,}000$ ft (Figure 2), Equation A6 yielded a value of 123 which is much greater than the 10.4 limit for nonviscous flow (i.e. the prototype is well into the nonviscous flow regime). From test 6 of this event, observed model data are $h_T = 0.1$ ft , $\Delta\rho_T = 0.00035$ g/cc , $\rho = 1.0000$ g/cc , $\nu = 10^{-5}$ ft^2/sec , and $\ell = 7.33$ ft ,

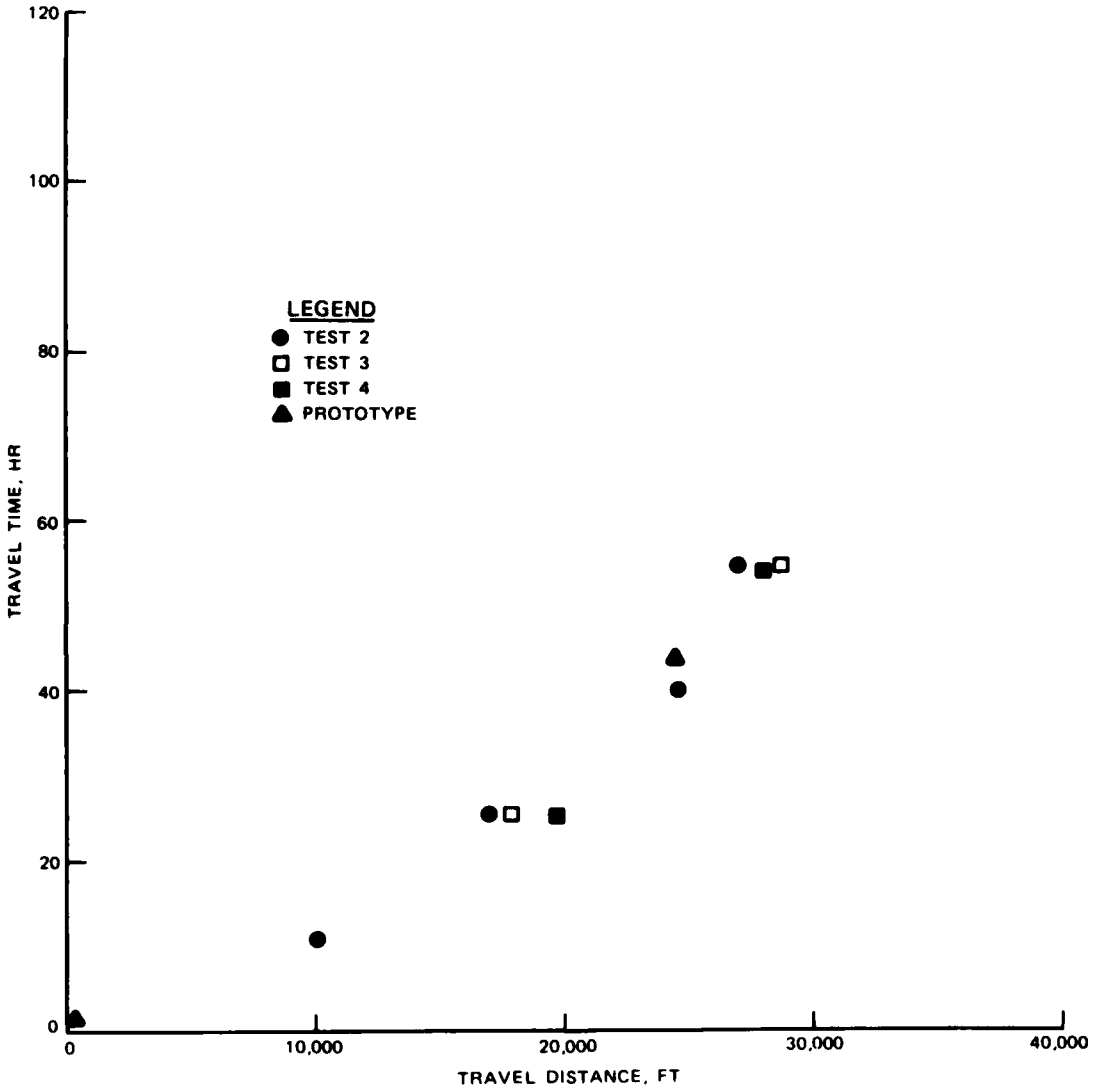

Figure 1. Density current travel distance versus time for the 29 March 1979 flood event

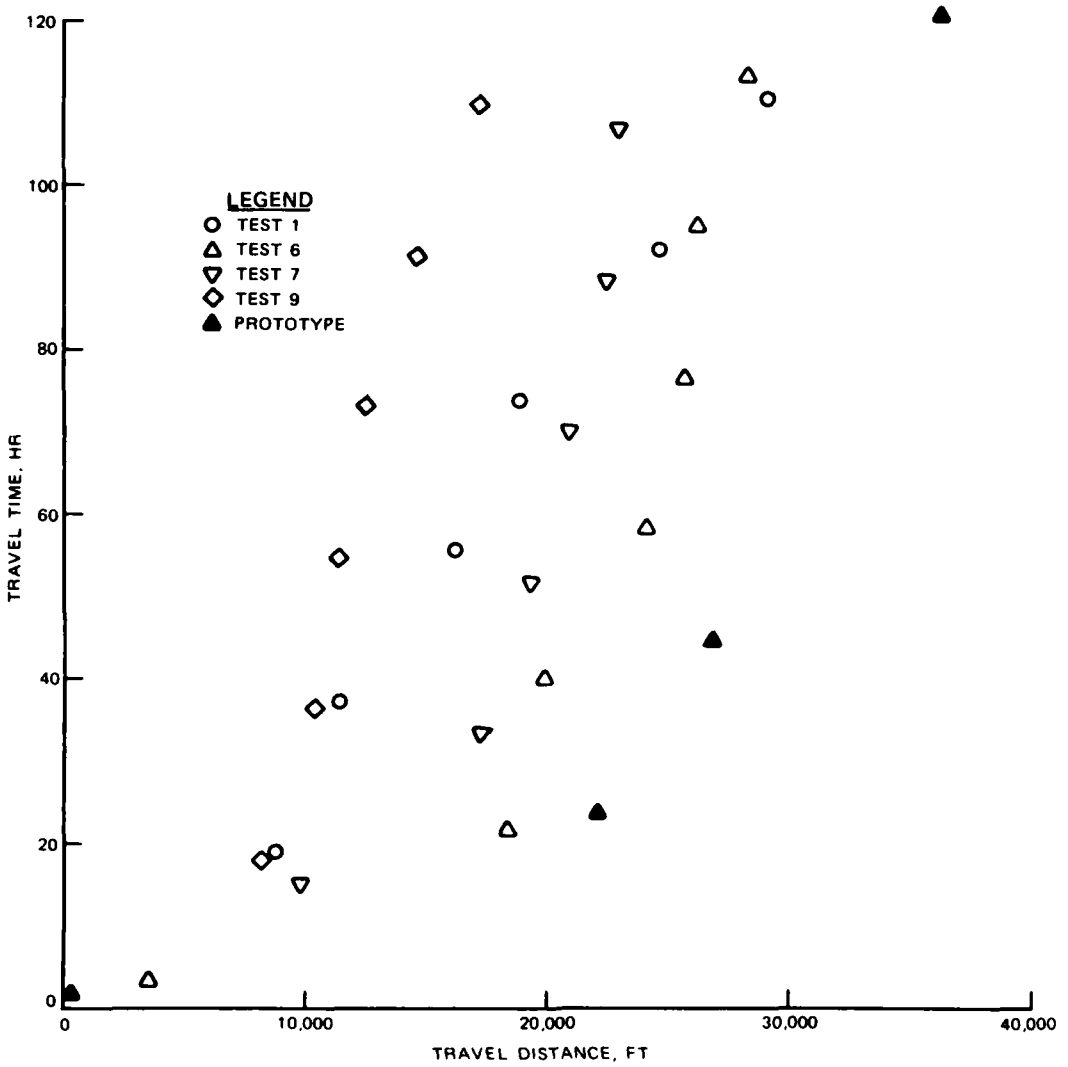

Figure 2. Density current travel distance versus time for the 14 November 1978 flood event

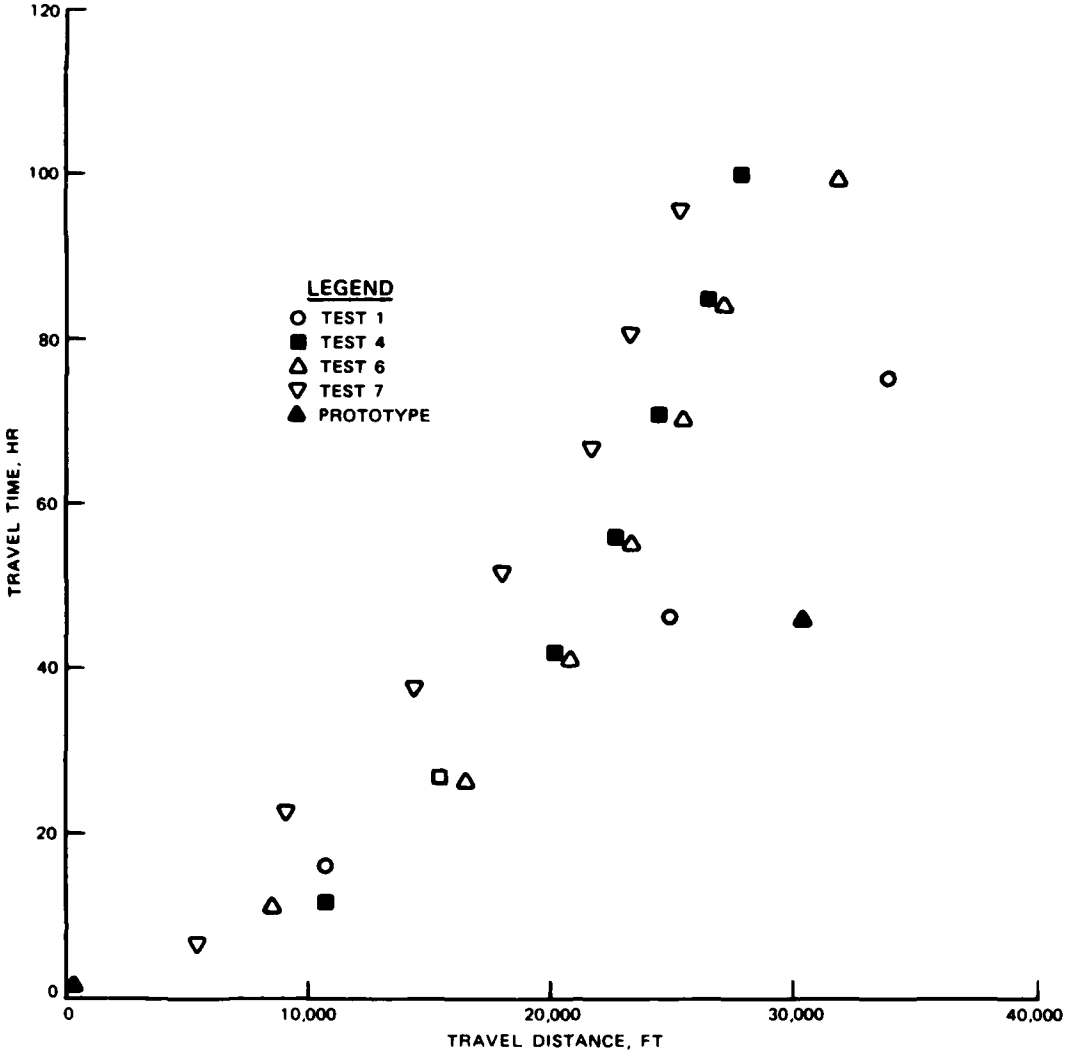

Figure 3. Density current travel distance versus time for the 24 October 1976 flood event

Equation A6 yielded a value of 5 for the model, indicating that the model inflow is in the viscous flow regime. Similar results were obtained for the 24 October 1976 event. Since the density current in the model was viscous-flow dominated, it would necessarily move slower than the current in the prototype.

45. It must be pointed out that the DeGray distorted physical model was constructed prior to acquisition of the prototype data for these density currents. The model was not designed to simulate these particular events. However, analyses of the results from each event indicated that the design was compatible with the large flood of March 1979 but not with smaller events of November 1978 and October 1976. Because the 29 March 1979 flood event was very large relative to the inflow of the other two events, the flow would remain nonviscous in the model and prototype for a much longer distance. Theoretically, only a large flood should reproduce well in the model since the distortion of this model is not within the criteria established in paragraph 28. The minimum distortion factor for this model based on Equation 25a and 25b should be 106.7; the actual distortion factor is 20.

46. For the 14 November 1978 flood event (Figure 2), a trend for density current travel time was observed in the model and prototype: the speed decreased as the current progressed through the lake. For the two other events, similar trends were observed in the model, although it was not evident from limited prototype data. The velocity decrease is due in part to three-dimensional effects. From the work of Manins (1976), for two-dimensional flow

$$C = 0.85\ (qN)^{1/2} \tag{32}$$

where the variables and stratification conditions are defined in Appendix A. For two-dimensional flow, the unit discharge q is the total inflow divided by the width of the current

$$q = \frac{Q}{W} \tag{33}$$

where

Q = total volumetric inflow rate

W = width of flow

For radial flow (Figure 4), the unit discharge q_r is given by

$$q_r = \frac{Q}{r\theta} \tag{34}$$

where θ = angle subtended by the arc at r. Thus, for radial flow, unit discharge is inversely proportional to the radial distance

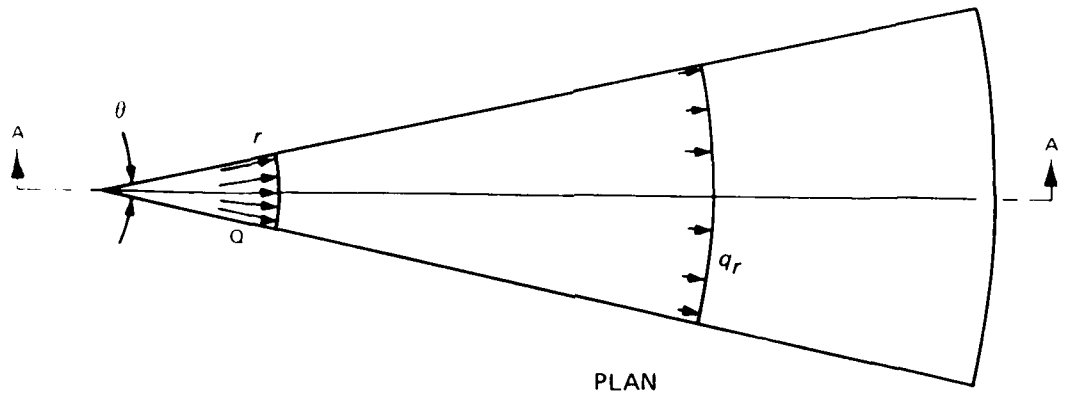

PLAN

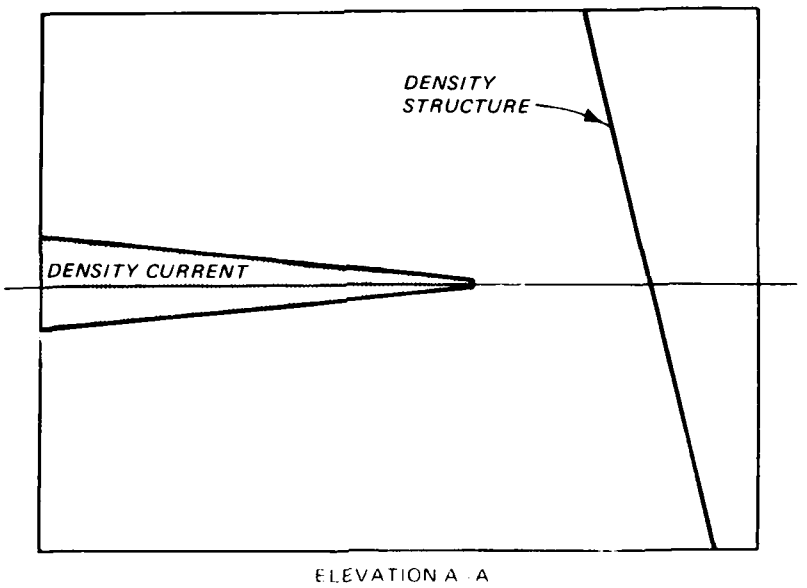

ELEVATION A - A

Figure 4. Radial flow

$$q(r) = \frac{Q}{r\theta} \qquad (35)$$

where $q(r)$ = unit discharge at radius r. From Manins' relationship and Equation 35, the intrusion velocity would also be inversely related to radial distance. Thus, the decrease in the speed of the density current in the model and prototype is at least qualitatively consistent with theory.

47. As can be seen in Figures 2-3, there is a large variability in model observations on presumably "replicate" tests of the events. The most probable cause of the differences from test to test is the difficulty in creating identical stratifications for each test coupled with model construction techniques. The model is made with "stepped" sides (Figure 5) to permit observation of current movement. The elevations of

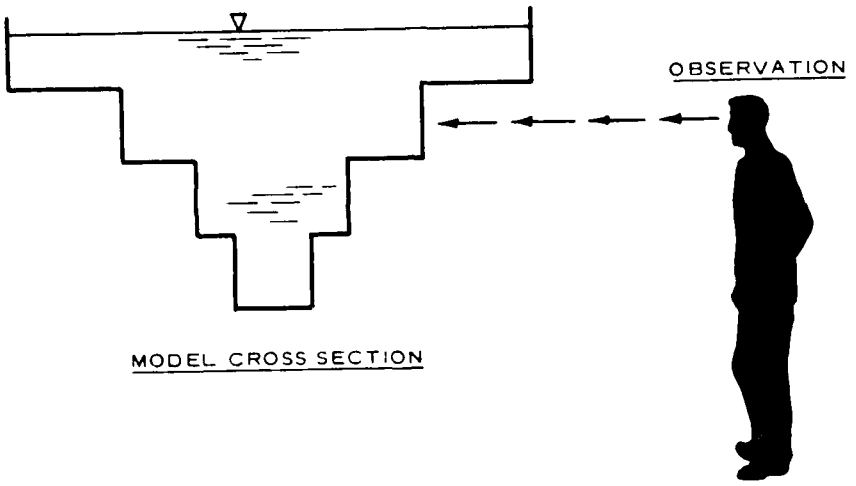

Figure 5. Stepped model construction for convenient observation

neutral bouyancy for the inflow currents of 14 November 1978 and 29 October 1976 were about el 367 ft and el 364 ft NGVD, respectively. A "step" in the model occurred at el 370. In relation to current thickness, the differences in the elevations of neutral bouyancy and step elevation are very small. If there were only a slight error in inflow density that raised or lowered the neutral bouyancy elevation in the model, the density current could experience dramatic differences in flow width, thereby

causing variation from test to test. Additionally, when modeling a specific inflow event, it is necessary to not only reproduce density differences but also the density gradient of the reservoir stratification. However, variability in replicate tests is not evident in Figure 1. The flood event on 29 March 1979 had a very large peak inflow. Because of the large flow rate, the current was very thick with an elevation of neutral bouyancy of 354. This tended to eliminate or mask the effects of small differences in vertical placement of the density current.

48. It can be concluded that thickness and resulting speed of the density current can be affected by viscous stresses, density structure, and model geometry. This does not imply that distorted physical model analyses cannot be effectively employed. Large flows may be simulated with a good degree of confidence, but small flows must be evaluated regarding the forces dominating flow movement to appropriately design the physical model to be used in their study.

49. GRH simulation. Data from the WES Generalized Reservoir Hydrodynamic (GRH) Facility was used as the prototype to make the second model-prototype comparison. The GRH is 80.0 ft long and 2.85 ft wide with a maximum depth of 3.0 ft. Details of the GRH are provided in Figure 6.

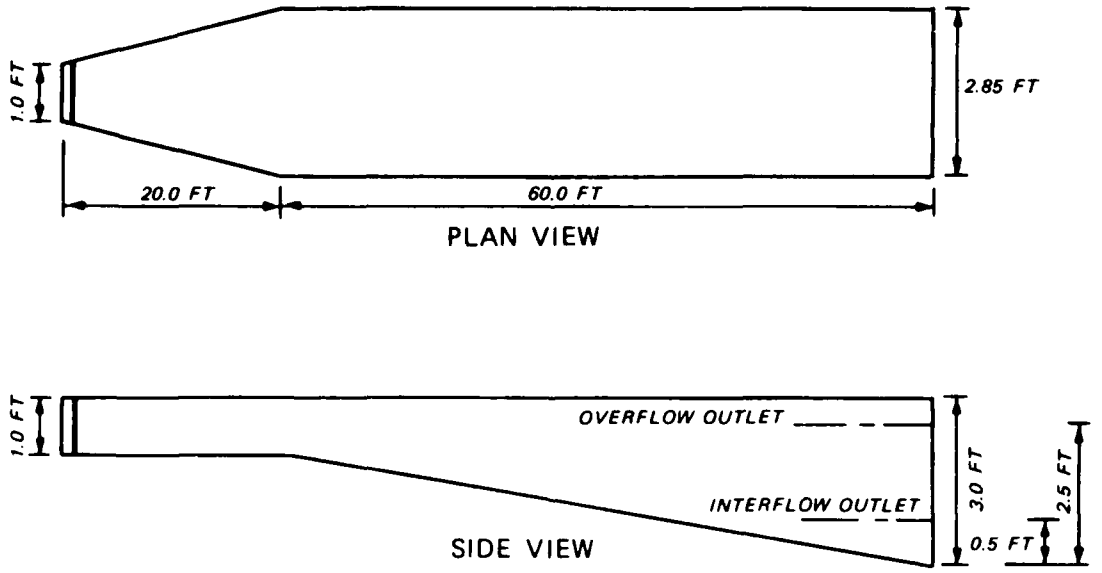

Figure 6. Schematic of GRH flume

50. Two conditions were simulated in the GRH: an interflow density current and an overflow density current. For both conditions, inflow was set equal to outflow with a flow rate of 10.0 gpm. The location of the outflow is shown for the two conditions in Figure 6. The inflow was baffled to distribute the flow uniformly from top to bottom. Supply water for the GRH can be heated or chilled to simulate desired density differences. For the interflow condition, thermal stratification was established in the GRH by spreading room temperature water on top of chilled water. Room temperature water was used for the upper layer of the ambient stratification in the interflow test to minimize surface heat transfer. An isothermal condition with chilled water was set up for the overflow case. Temperature profiles are shown in Figure 7 for the two conditions. Chilled water was warmed and automatically controlled to provide a steady-state inflow temperature of 62.0° F for the interflow condition. Room temperature inflow water at 72.0° F was used for the overflow case. This minimized the surface heat transfer of the overflow density current. However, since the ambient water was chilled, it was possible for the ambient water to warm slightly during the test.

51. The inflows were dyed so intrusion length and thickness (at various stations) could be visually determined. Additionally, the elapsed time from the beginning of inflow and outflow was recorded. The same type of data was collected from the distorted model so that a direct comparison could be made with the prototype (GRH).

52. The prototype-to-model horizontal and vertical length scale ratios were 15.0 and 1.5, respectively, giving a distortion factor of 10.0. The model was stratified with saline and fresh water to provide the same density difference as that caused by thermal stratification for the GRH interflow condition. Similarly the salinity of the model inflow was adjusted to provide an inflow density difference (with respect to ambient stratification) equal to that of the GRH interflow condition. For the model overflow case, a freshwater inflow and saline receiving water were used, again maintaining prototype density difference.

53. The two inflow conditions were simulated with the model and

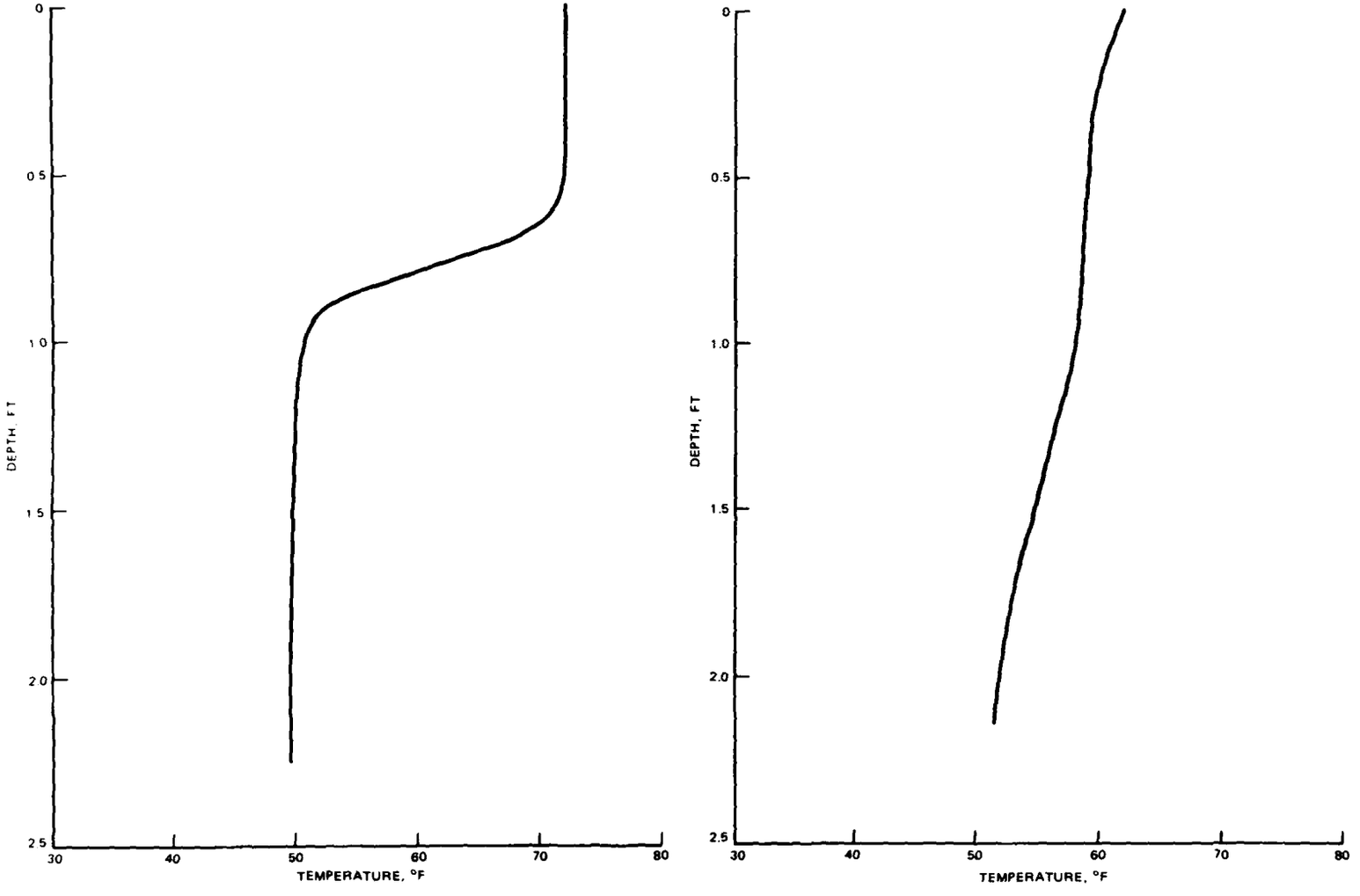

a. Interflow

b. Overflow

Figure 7. GRH thermal stratification

two types of comparisons were made. Density current travel time or intrusion length versus time was compared for the model and GRH, and intrusion vertical thickness was compared at various longitudinal stations for the same intrusion length. The comparison of model-prototype travel time for the interflow case is shown in Figure 8. Because of difficulty in establishing the origin for elapsed time in the GRH and model (due to unequal inflow entrance conditions), all times are referenced to the time when the intrusion reached the 1/8 station (or traveled 10.0 ft of the GRH length). The model travel time compares closely with that of the GRH except when the intrusion reaches the end of the flume. It is not clear why the GRH interflow slows down at the dam. This may be due either to the beginning of viscous effects or to an internal wave (seiche) reflecting off the dam (flume wall) as the interflow is arriving, thus slowing the interflow speed. Seiche action in the model may be damped or out of phase with the GRH. In general, scale models with length scale distortion can be used to model long waves but cannot be used to model short waves (LeMéhauté 1976). Thus, it is possible for internal waves of short length to be out of phase in the distorted model compared with the GRH. The GRH and model intrusion elevation and thickness (Figure 9) are similar. The major difference between them is that the GRH interflow experienced a peak thickness where the model interflow had a dip (at mid-length). Again the difference may have been due to unequal damping of internal waves and some internal wave phase shift.

54. Inspection of Figure 8 indicates the GRH interflow is a nonviscous intrusion for $\ell \leq 70$ ft . Solving the following equation (Equation A6) for $h_T \simeq 0.275$ ft , $\Delta\rho_T = 0.00163$ g/cc , $\rho = 1.0$ g/cc , $\ell = 70.0$ ft , and $\nu = 10^{-5}$ ft^2/sec , results in

$$\frac{h_T^{5/2} \sqrt{\frac{\Delta\rho_T}{\rho} g}}{\nu\ell} = 12.9 \qquad (36a)$$

Since this value is greater than 10.4, the intrusion is in the nonviscous regime. For the distorted model

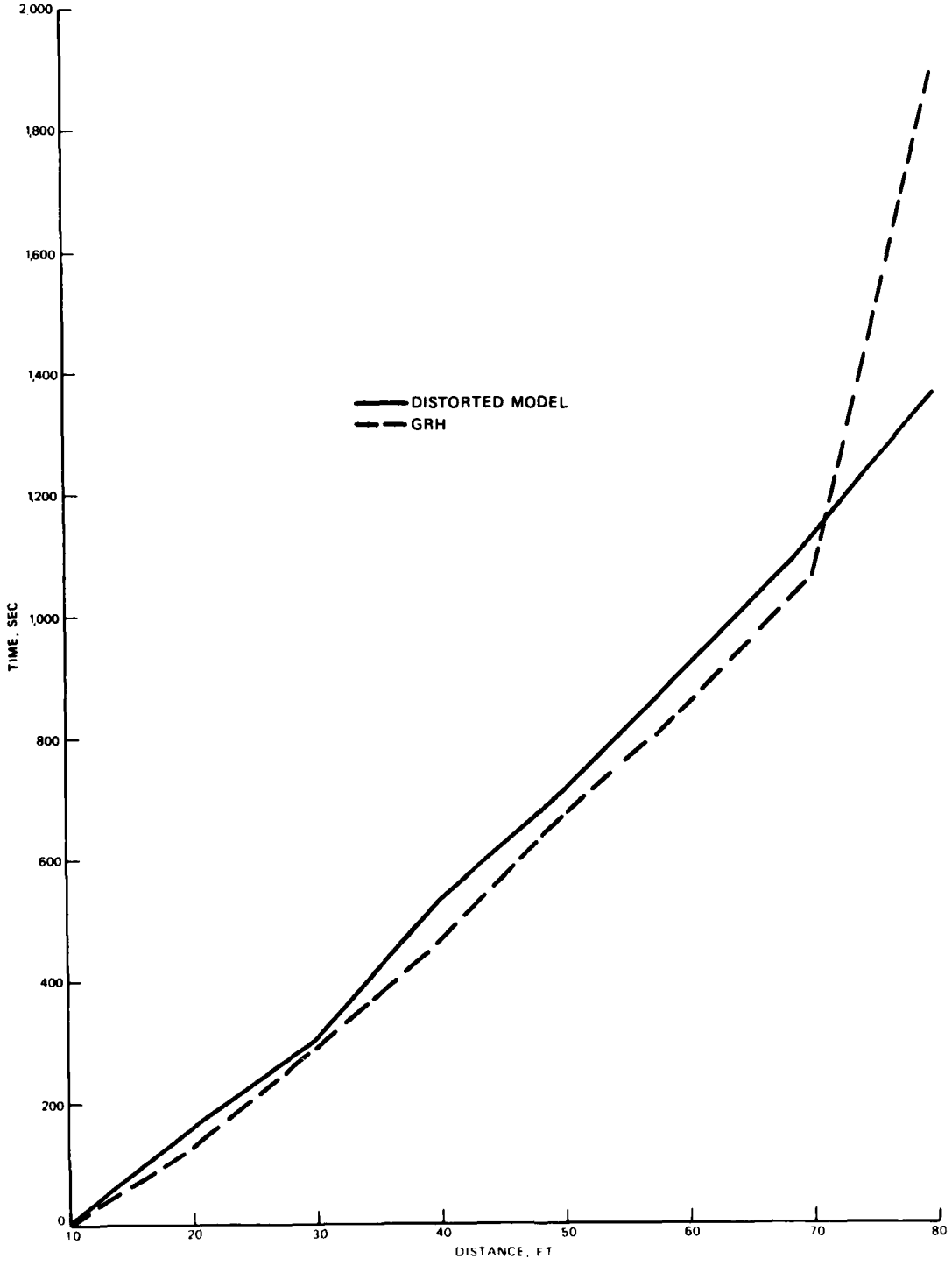

Figure 8. Interflow density current travel time

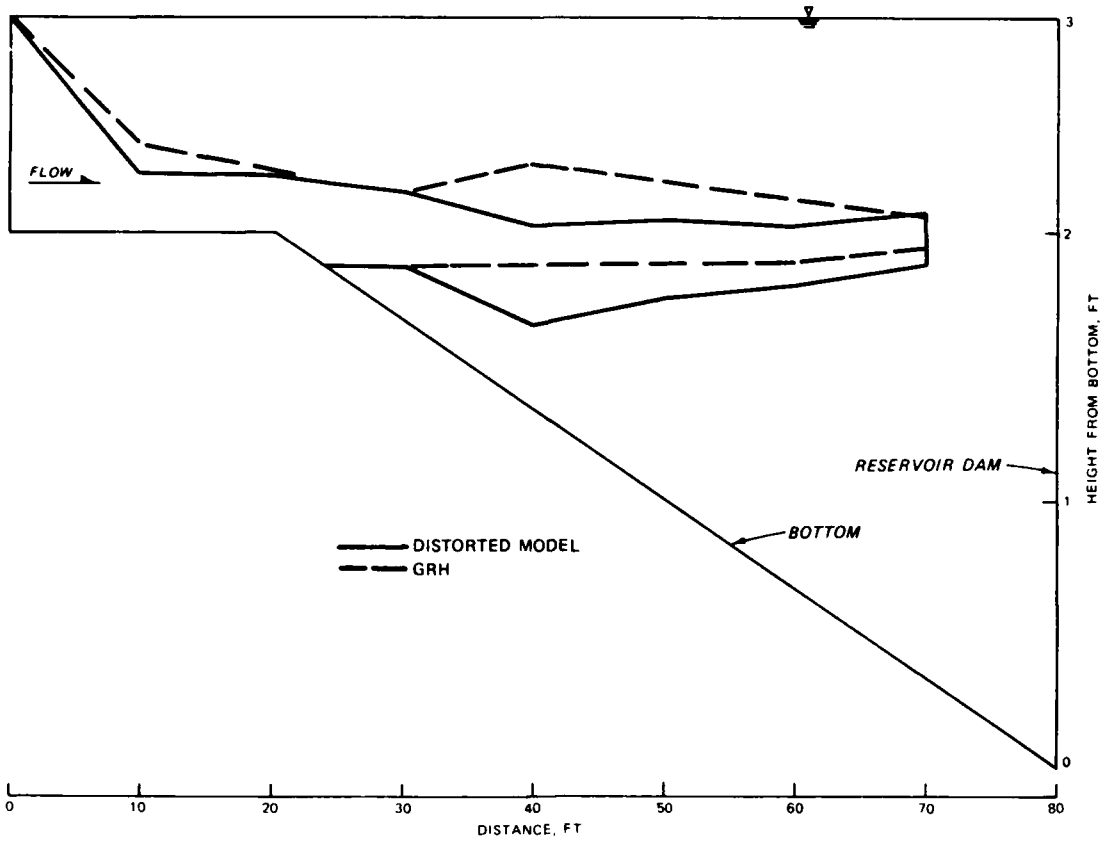

Figure 9. Interflow density current thickness

$$\frac{h_T^{5/2} \sqrt{\frac{\Delta\rho_T}{\rho} g}}{\nu \ell} = 71.1 \qquad (36b)$$

for the same intrusion length. Therefore the model intrusion is also well into the nonviscous range. This is not surprising since the distortion factor was greater than that specified by Equation 25. Clearly, the intrusion speed and thickness were adequately reproduced in the model as both the model and GRH intrusions were in the nonviscous range for most (at least $\ell \leq 70.0$ ft) of the test.

55. It is worth noting that the use of Equation A4 (paragraph A6, Appendix A) to predict the intrusion thickness resulted in $h_T = 0.31$ ft compared to h_T observed of about 0.275 ft. Using the observed $\Delta\rho_T$ of 0.00163 g/cc and h_T of 0.275 ft, the intrusion speed computed from

Equation A2 is $c = 0.060$ ft/sec as compared with that observed of $c = 60/1060 = 0.057$ ft/sec. Thus, the use of Equations A4 (or A5) and A2 seems to be appropriate for an approximation of the interflow characteristics.

56. Comparisons of GRH and model overflow density current data are shown in Figures 10 and 11. The model travel time compares closely with that observed in the GRH. The current thickness in the model is not as great as that observed in the GRH. The difference may be due to a greater degree of vertical diffusion in the GRH than in the model. This reasoning is in agreement with the discussion in paragraph 32.

57. The observed thickness of the GRH overflow density current was about 0.15 ft and the density difference was approximately 0.0012 g/cc. With these values, the nonviscous range according to Equation A9 exists for $\ell \leq 18$ to 35 ft. Examination of Figure 10 indicates that the GRH overflow is nonviscous for at least the first 60 ft. After traveling

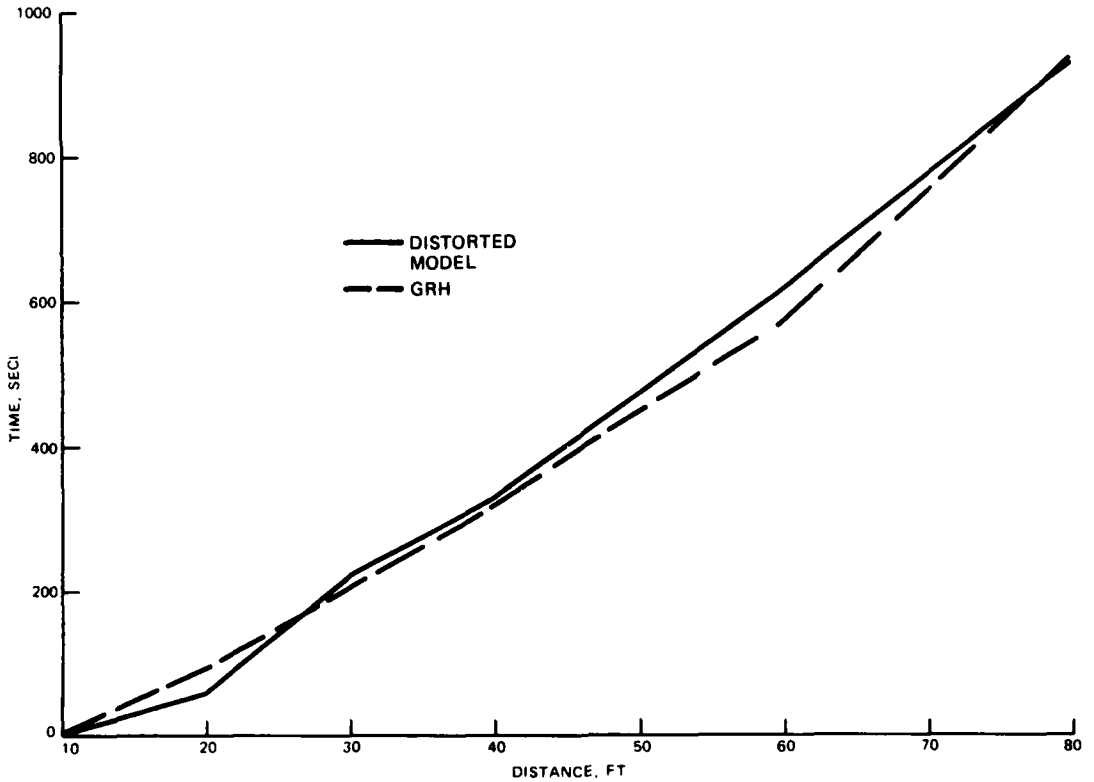

Figure 10. Overflow density current travel time

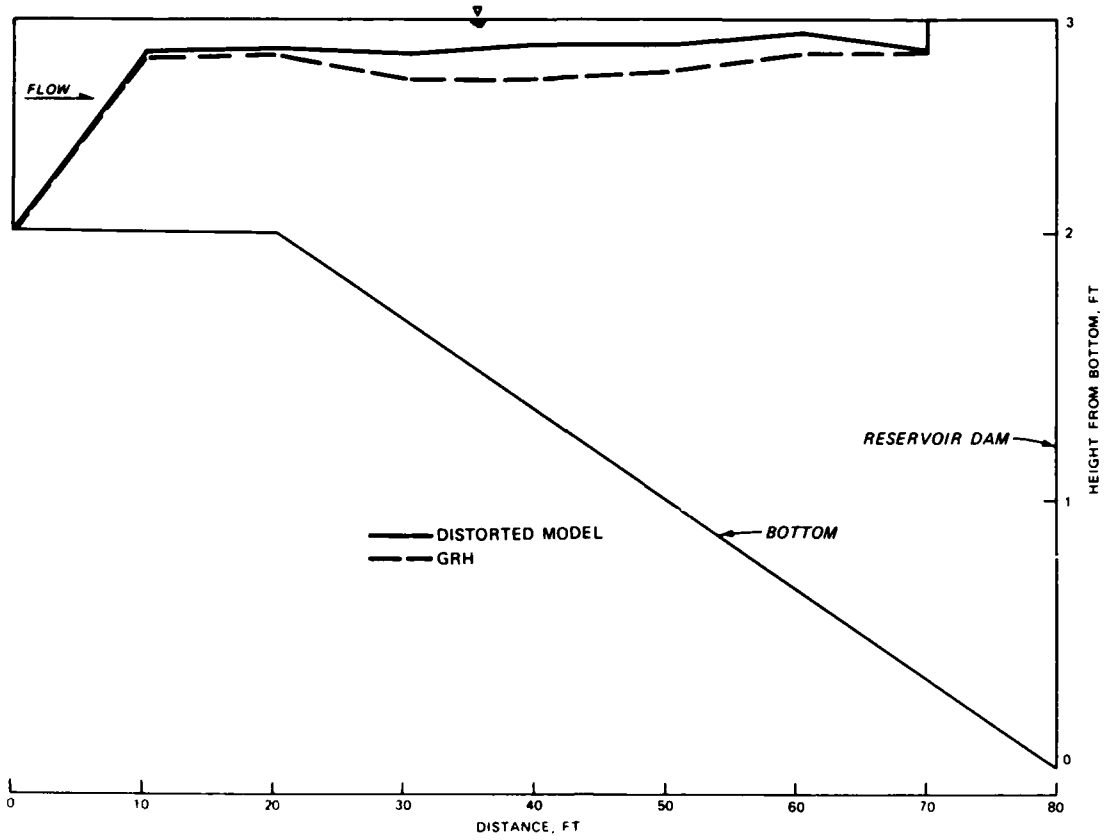

Figure 11. Overflow density current thicknesses

a distance of 60 ft, the GRH travel time plot curves upwards possibly due to viscous effects. The curve is almost straight for the first 60 ft indicating that the flow must be in the nonviscous range for $\ell \leq 60$ ft. This suggests that the value for the right side of Equation A9 may be too high. The model overflow was computed to be in the nonviscous range throughout. The density current thickness h_K, as computed from Equation A8, is 0.14 ft compared with about 0.15 ft observed. Use of Equation A7 results in a computed c of 0.067 ft/sec compared with that observed of $c = 40/470 = 0.085$ ft/sec. This fairly good agreement indicates that Equations A8 and A7 may provide a good first approximation of overflow thickness and speed for the nonviscous range. Again the distorted model agrees relatively well with the GRH since the physical process is primarily Froude number related and the model is Froudian.

Hydraulic destratification

58. A design technique for lake hydraulic destratification was

reported by Dortch (1979) and Holland and Dortch (1984). In hydraulic destratification, water jets are used to induce mixing (Figure 12).

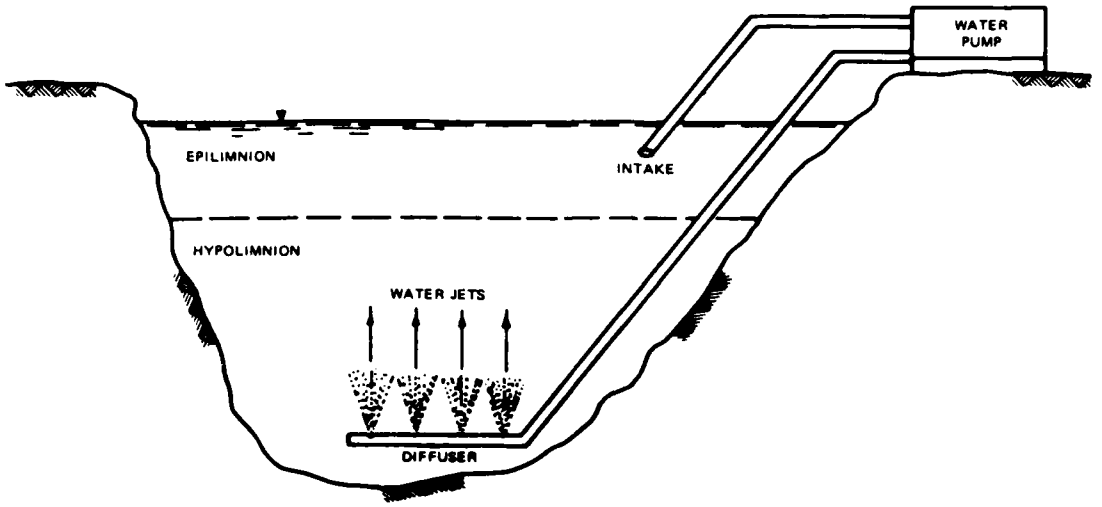

Figure 12. Cross-sectional view of a reservoir hydraulic destratification system

Although there are several physical processes that contribute to mixing, such as entrainment into a buoyant jet/plume and subsequent spreading of the flow as an intrusion, it was found that the rate of mixing could be expressed as a function of the densimetric Froude number, or

$$\frac{t_{80\%}Q}{V_L} = 0.204\left(\frac{V}{\sqrt{\frac{Z\Delta\rho}{\rho}\, g d_L}}\right)^{-0.57} \tag{37}$$

where

$t_{80\%}$ = elapsed pumping time to reach 80 percent totally destratified

Q = pumping rate

V_L = total lake or reservoir volume

V = exit velocity of water jets

$\Delta\rho$ = density difference of hypolimnion and epilimnion

ρ = density of epilimnion

d_L = depth from lake water surface to diffuser

This result was determined through an experimental program at WES using laboratory tanks (see paragraphs 71-72). Turbulent flow was maintained for all tests, and the flow rate, jet velocity, and reservoir depth, volume, shape, and density stratification were varied over a wide range so that the results should be applicable to the field condition.

59. A study was conducted to determine if the effectiveness of a design using this type of destratification system could be evaluated on a site-specific basis with a hydraulic model. If so, site-specific model studies to improve candidate systems would be desirable prior to field installation. Of course, for practicality and preservation of turbulent flow, the lake model would have to be vertically exaggerated. A primary concern was whether the mixing process could be modeled properly with a distorted model. It was thought that a vertically exaggerated Froudian model could properly simulate this type of destratification because the mixing process was dependent on a densimetric Froude number. However, the mixing process depends on near-field entrainment and far-field convective spreading so there was some question as to whether a distorted model could properly model these effects simultaneously and how to size the model diffuser.

60. Because there were no field data on this type of mixing process, tests previously conducted in a laboratory tank had to be considered prototype data and a distorted-scale model of the tank was built. Two tests conducted with a 20-ft-square, 2.0-ft-deep tank were selected for study. The details of these tests are summarized below:

Parameter	Test No. 1	Test No. 17
Q, gpm	2.0	3.0
D, in.	1/2	1/2
V, fps	3.27	4.90
V_L, ft^3	520.0	720.0
d_L, ft	1.3	1.8
$\Delta\rho$, g/cc	0.0036	0.0022

where D is the port diameter of the single-port diffuser that was used.

61. A distorted model of the tank was constructed at a scale of $X_R = 20.0$ and $Y_R = 2.0$. As before $\Delta\rho_R = \rho_R = 1.0$. V_m and Q_m were scaled according to Froudian scaling criteria and D_m was sized to give the proper V_m given Q_m. For the model, the properly scaled test conditions were:

Parameter	Test No. 1	Test No. 17
Q, gph	2.12	3.18
D, in.	5/64	5/64
V, fps	2.31	3.46
V_L, ft^3	0.65	0.90
d_L, ft	0.65	0.90
$\Delta\rho$, g/cc	0.0036	0.0022

The performance of the mixing systems was measured by plotting the percent of total destratification versus pumping time. The percent of total destratification is calculated from the change in the stability of the stratification which is obtained by density measurements as explained by Dortch (1979). Because the percent of total destratification is dimensionless, it is not necessary to scale those numbers from model to prototype. Of course, model pumping time had to be scaled to prototype values.

62. The performance plot for test No. 1 is shown in Figure 13 with model and prototype values indicated. It is apparent from this plot that the model simulated the prototype very closely. When model test No. 17 was run, however, it was found that the model mixed much too quickly. The model depth was 0.90 ft for this test, which is almost the same as the length and width of the model tank. With the available distance for vertical and lateral spreading, it was considered that there might be wall effects that could influence the rate of mixing. Thus, a larger vertical scale ratio was tried. Using the model depth of test No. 1 of 0.65 ft for test No. 17 resulted in a vertical scale factor of $Y_R = 1.8/0.65 = 2.77$ rather than $Y_R = 2.0$. This resulted in a DF of 7.22 rather than 10.0. The No. 17 test conditions then became:

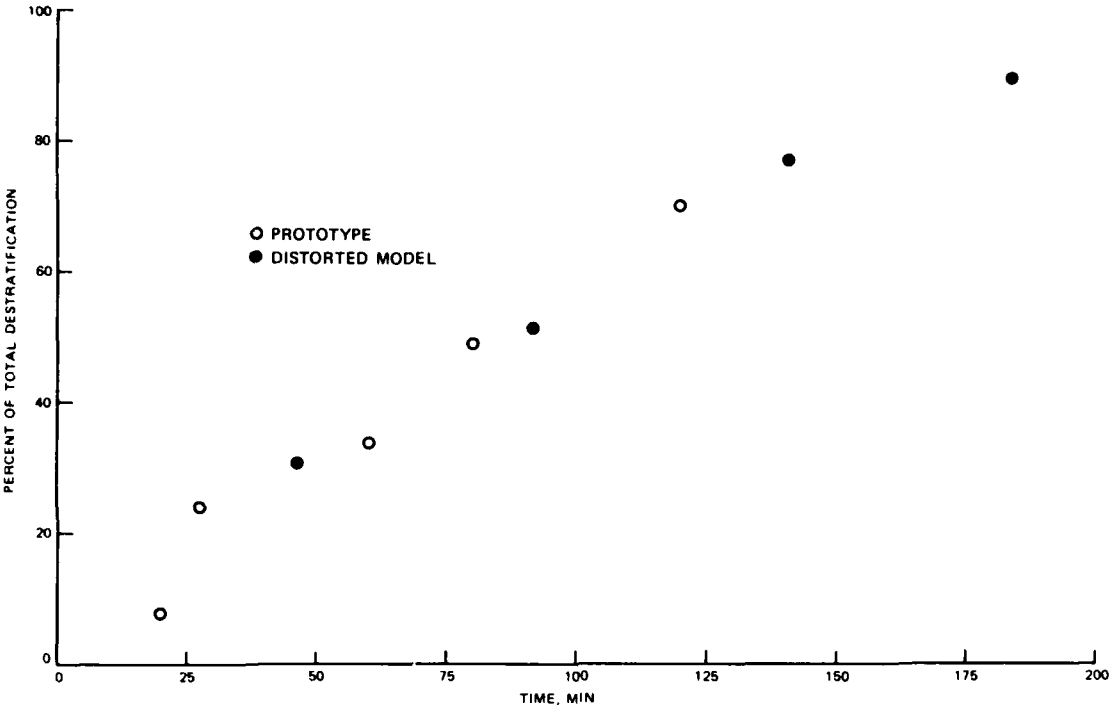

Figure 13. Destratification performance, test No. 1

Parameter	Value
Q, gph	1.95
D, in.	1/16
V, fps	2.94
V_L, ft^3	0.65
d_L, ft	0.65
$\Delta\rho$, g/cc	0.0022

This adjustment proved to be successful as can be seen by the close comparison of model and prototype data shown in Figure 14. These results indicate that this type of destratification system can be simulated fairly well with a Froudian distorted length scale model as long as lateral mixing is not inhibited by the model walls. If the distortion factor is too large, the model walls may artificially influence the mixing process.

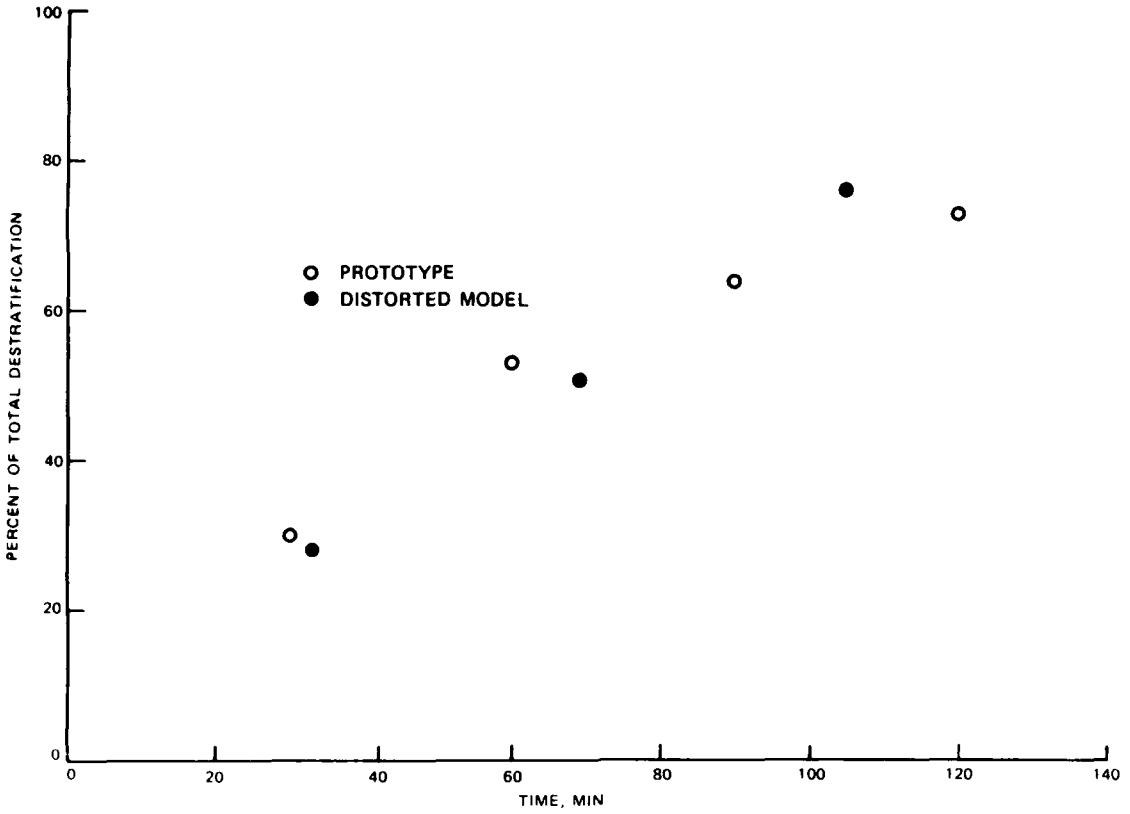

Figure 14. Destratification performance, test No. 17

63. Sizing the diffuser for a multiport diffuser of a hydraulic destratification project would be done in the same manner as referenced in paragraph 34. The port size and spacing would be scaled by the vertical scale and the number of ports would be reduced by the distortion factor. This would still give the proper V_m for a given Q_m.

PART IV: EXAMPLE APPLICATIONS OF PHYSICAL MODELS OF RESERVOIRS

64. Employing much of the information discussed in previous parts, several general research projects and site-specific investigations have been conducted at WES using physical models of reservoirs. The Bibliography provides a publications list of reports on studies using physical models of reservoirs. Several examples are described below.

Selective Withdrawal Research

65. Mathematical descriptions of the selective withdrawal phenomenon have been analytically and experimentally developed by several researchers i.e., Bohan and Grace (1969). Simple geometries and general (nonspecific) conditions have been and are being used to develop and enhance the existing knowledge about selective withdrawal. Studies on specific project models have, in many cases, verified or enhanced existing mathematical descriptions for selective withdrawal. Research designed to refine and enlarge the applicability of existing mathematical descriptions continues to be conducted at WES using small-scale laboratory facilities. The dimensionless relationships developed from these studies allow the application of model results to prototype situations.

66. Selective withdrawal investigations are conducted in a large flume (Figure 15) designed specifically for selective withdrawal research. Stratification similar to that expected in reservoirs and lakes is established by slowly floating fresh water over saltwater. This procedure creates the epilimnion and hypolimnion. Water is released through a port, over a weir, or via other outlet devices and the resulting velocity distribution and withdrawal zone (Figure 16) are determined using "dye streak" flow visualization techniques. The dye streak is displaced toward the outlet as water is withdrawn and the withdrawal distribution is determined from the time rate of displacement. The streak's displacement is recorded on video tape allowing stop-action analysis of the withdrawal zone dimensions.

67. Ongoing studies are being conducted to evaluate the

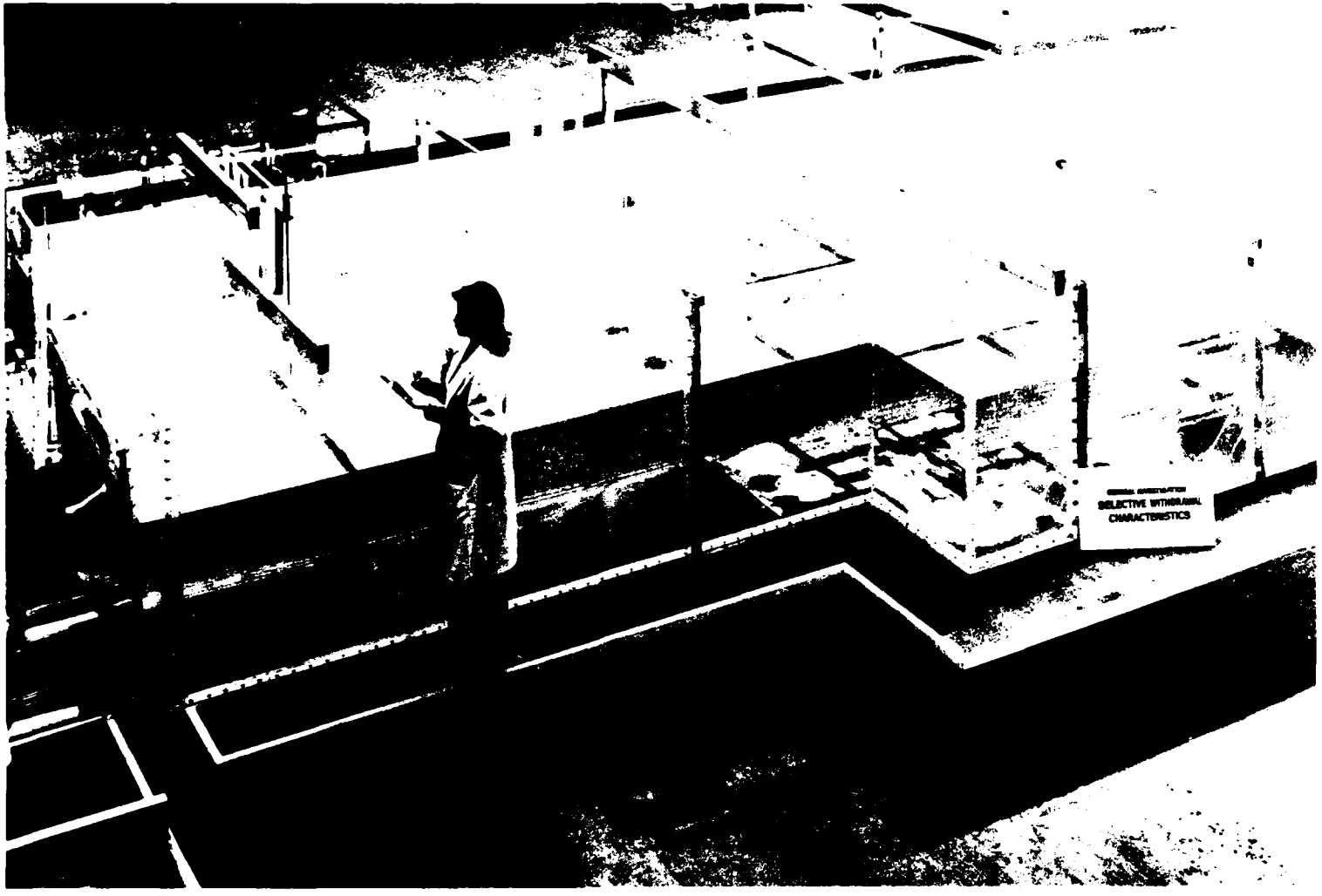

Figure 15. Selective withdrawal test flume

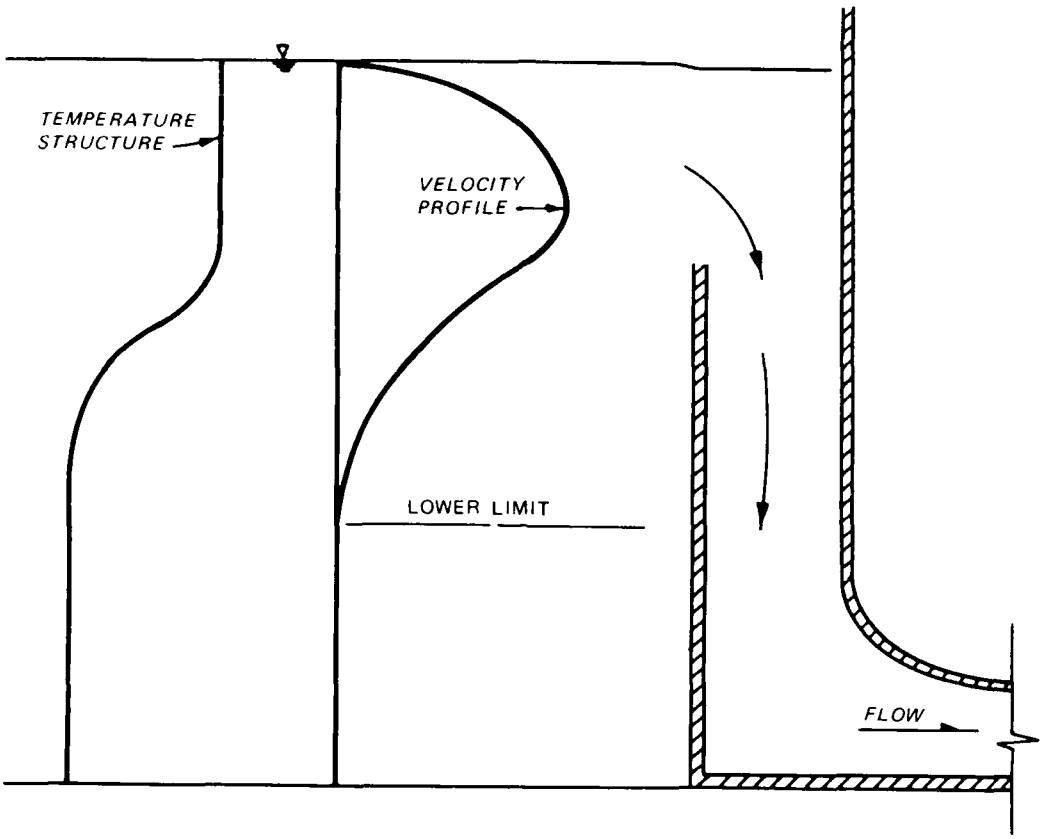

Figure 16. Selective withdrawal over a weir

withdrawal characteristics of various outlet configurations. The effects of port dimensions (vertical and horizontal extent of opening), partially submerged ports, and submerged sharp crested weirs with various heads and weir lengths are being studied. The investigation should result in the development of criteria that define the flow regime over which existing selective withdrawal predictive techniques are applicable and should also result in improvements in the mathematical descriptions.

Dickey-Lincoln School Lakes Model

68. Dickey-Lincoln School Lakes is a pumped-storage hydropower project proposed by the New England Division for Maine. An undistorted near-field model of Dickey Lake outlet geometry (outlet structure and

local topography) was constructed to study the withdrawal and pumpback mixing characteristics unique to the Dickey Lake inlet-outlet structure (Dortch, Fontane, and Wilhelms 1976). The model reproduced the structure and upstream topography for a prototype area of about 3,600 ft square (Figure 17). It was constructed to a scale of 1:200, which resulted in the following scale relationships based on Froudian modeling criteria for transferring model data to prototype equivalents.

Dimensions	Scale
Length (prototype:model)	200
Velocity	14.14
Time	14.14
Volume flow rate	565,685
Density difference	1

69. The model was used to determine if the vertical distribution of withdrawal could be predicted from the generalized mathematical selective withdrawal description (Bohan and Grace 1973) and to provide withdrawal information if modifications to the mathematical description were required. The model was also used to evaluate the gross entrainment, mixing, and dilution characteristics of the pumpback jet.

70. The investigation resulted in these revisions to the generalized mathematical selective withdrawal description: (a) reduction of effective weir length to force a lower limit of withdrawal, (b) lowering of the predicted elevation of maximum velocity, and (c) modification of the equation that predicts velocity distribution. These changes were site specific and attributed to the effects of local topography. Pumpback was also studied in the model and entrainment was evaluated. A computer algorithm, based on these results, was developed to account for the mixing characteristics of pumpback. The selective withdrawal modifications and the pumpback algorithm were interfaced with the one-dimensional (vertical) mathematical thermal reservoir model WESTEX (Holland, Dortch, and Smith 1982) for simulation of the spring through fall seasons.

Figure 17. Dickey Lake near-field undistorted model

Reservoir Destratification

71. Artificial destratification of reservoirs is one of several alternatives for increasing the dissolved oxygen (DO) content in the lower levels of a reservoir. Usually, thermal/density stratification in a reservoir impedes the transport of oxygen from the surface to the bottom of the reservoir. As a consequence, the hypolimnion may become anaerobic resulting in dissolution of trace metals, release of nutrients that may stimulate eutrophication, formation of hydrogen sulfide, and depression of pH. If sufficient mixing energy can be artificially introduced to the reservoir, existing stratification can be eliminated allowing complete mixing and transport of DO to the lower levels of the reservoir, thus maintaining DO and avoiding the effects of anaerobic conditions.

72. Research has been conducted by Dortch (1979) and Holland and Dortch (1984) to determine the design parameters and provide guidance to produce an effective means for artificially destratifying lakes using hydraulic methods (pumping water). Laboratory tanks of various sizes and shapes were used to simulate stratified reservoirs to develop dimensionless parameters that describe the destratification process. A dimensionless description of the mixing phenomena observed in the model studies was developed from which the average velocity required to mix a given reservoir in a specified time period for a given stratification and pumping rate could be predicted. These results can be used in the planning, preliminary design, and evaluation of a hydraulic system for destratification of a reservoir.

Marysville Lake Hydrothermal Study

73. This study was conducted to determine the ability of the proposed Marysville Lake pumped-storage project (California) to satisfy downstream water temperature objectives (Fontane et al. 1977). The study required (a) an understanding and description of the large-scale hydrodynamic phenomena within the project, (b) development of expected

temperature profiles within Marysville Lake, and (c) estimation of temperatures released from Marysville Lake and from the afterbay. A physical hydrodynamic model and a numerical simulation model were used in the study. The distorted-scale physical model provided information about the hydrodynamic response of Marysville Lake for various operational conditions. The numerical model provided the capability to assess, for year-long periods, the effect of historical meteorologic and hydrologic data and various operating conditions on temperature regimes within and downstream of the project.

74. The distorted-scale model was used to evaluate the effects of the morphology and the unsteady generation and pumpback operations on the density stratification of Marysville Lake and afterbay and to help identify, validate, and quantify modifications to the mathematical model that would improve the reliability of the predictions. The physical model (Figure 18) was constructed to a distorted length scale ratio of 1:160 vertically and 1:1,600 horizontally. Through vertical scale distortion it was possible to preserve turbulent flow while simulating the entire reservoir and afterbay. Although the level of distortion chosen did not conform to the criteria given in Equations 25a and b for the maintenance of the nonviscous spreading regime, the processes of interest (i.e., entrainment) were dominated by inertial rather then viscous forces. Thus, the chosen distortion factor did not compromise the model results. With the density differences in the model set equal to those in the prototype, the accepted equations of hydraulic similitude based on Froudian relations (paragraph 17) were used to express the mathematical relations between the dimensionless and hydraulic quantities of the model and the prototype. Allowing for vertical scale distortion, the general relations for transfer of model data to prototype equivalents were as follows:

Dimension	Scale Relation
Length in vertical direction (prototype/model)	160
Length in horizontal direction	1,600

(Continued)

Figure 18. Marysville Lake distorted-scale hydrodynamic model

Dimension	Scale Relation
Area in vertical plane	256,000
Area in horizontal plane	2,560,000
Velocity	12.65
Time	126.5
Flow	3,238,172
Density difference	1

75. It was determined from the physical model study that the pumpback density current had a much stronger effect on lake stratification than inflow or withdrawal. Inflow to the reservoir was found to affect the thermal structure of the lake in a very short time, usually within a week, for normal river flows. It was also determined that, due to geomorphometry of the reservoir, a large volume of the hypolimnion would not be mixed during pumpback and would not be released during generation. A high ridge between the dam and the Dry Creek arm of Marysville Lake prevented the cold (hypolimnion) water in the Dry Creek arm from being mixed or withdrawn. This decrease in coldwater storage had to be accounted for in the numerical simulations. Additionally, the amount of mixing in the afterbay was estimated with the physical model and these results were incorporated into the numerical model. The modifications made to the numerical model helped account for some of the hydrodynamic and geomorphological effects expected to occur in the lake and afterbay and provided better estimates of the thermal regimes within and downstream of the project.

PART V: SUMMARY

76. This report provides guidance for the use of physical models to study reservoir hydrodynamics. Modeling theory is developed by examining the Navier-Stokes equations of fluid motion. These equations are nondimensionalized resulting in fluid motion equations containing the Froude and Reynolds numbers. These equations are used to develop the relationships of model-to-prototype forces. This requires that the model Froude and Reynolds numbers be equal to prototype Froude and Reynolds numbers, respectively, thereby providing complete dynamic similarity.

77. Upon closer scrutiny, complete dynamic similarity is not feasible if ordinary fluids are used in the modeling process. In other words, if water is the model and prototype fluid, the equivalence of the model Froude and Reynolds number and prototype Froude and Reynolds cannot be preserved. This distortion from complete similitude does not, however, invalidate physical modeling. Rather, it places a constraint on modeling that must be considered during model development. For free-surface flow regimes such as reservoirs, modeling on the basis of the Froude number can provide accurate similitude if the model Reynolds number indicates that the flow is of the same fundamental character (turbulent) as the prototype. Thus, the constraint noted in the previous paragraph may be overcome by selecting an appropriate length scale for the model.

78. Scale relationships based on equating the model and prototype Froude numbers are developed for undistorted- and distorted-length scale models. From these relationships, the ratio of prototype-quantity-to-model-quantity can be determined. Thus, distance, time, velocity, and flow rate may be scaled for transfer from model to prototype or prototype to model.

79. Examples of applying these relationships and the distorted- and undistorted-scale modeling concepts are presented. Several studies are briefly discussed and important results of the physical model studies are presented. In many instances, observed hydrodynamic processes were mathematically described for incorporation into a numerical hydrodynamic,

thermal, or withdrawal model. In other cases, observations improved the credibility of numerical predictions.

80. Undistorted- and distorted-length scale modeling of reservoir inflow, outflow, density currents, jets, and dispersion is discussed. Criteria for sizing distorted models are presented. Effects of length scale distortion on reservoir hydrodynamic processes are discussed. Recommendations are made regarding application of these modeling techniques to stratified flow phenomenon in reservoirs. Froudian models without length scale distortion should be used to physically model near-field reservoir hydrodynamics which would include studies for selective withdrawal and buoyant jet diffusion. Physical model studies of far-field reservoir hydrodynamics require length scale distortion for economy of size, preservation of turbulent flow, and to compensate for excessive interfacial shear.

81. Viscous and inertial forces play important roles in the movement of water in a prototype or a model. Intuitively, to correctly simulate these forces, a model should reproduce the same conditions as in the prototype. For instance, if a density current in the prototype is in a nonviscous flow regime (nonviscous spreading), then the model current must also be in nonviscous flow. Criteria were developed that indicate whether the flow is viscous or nonviscous. Distorted model-prototype comparisons are made for density current advection. The results verified that nonviscous spreading of a density current in the prototype can be satisfactorily simulated with a Froudian distorted-length scale model as long as the model density current is also in the nonviscous flow regime. It is also demonstrated that hydraulic destratification of a reservoir, which is a Froudian process, can be modeled very satisfactorily with a distorted scale model.

82. In many cases, results from near-field flow models can be coupled with far-field distorted-length scale models; often, however, it is necessary to make adjustments in the distorted model to the near-field process. Furthermore, when modeling far-field flow processes that are dominated by viscous effects and turbulent diffusion, Froudian distorted-length scaling is necessary but will not ensure similitude.

Model flow inhibitors, such as roughness strips, may be required to reduce transverse mixing and increase vertical mixing.

REFERENCES

Bohan, J. P., and Grace, J. L., Jr. 1969. "Mechanics of Flow from Stratified Reservoirs in the Interest of Water Quality; Hydraulics Laboratory Investigation," Technical Report H-69-10, US Army Engineer Waterways Experiment Station, Vicksburg, Miss.

Bohan, J. P., and Grace, J. L., Jr. 1973. "Selective Withdrawal from Man-Made Lakes; Hydraulic Laboratory Investigation," Technical Report H-73-4, US Army Engineer Waterways Experiment Station, Vicksburg, Miss.

Dortch, Mark S. 1979. "Artificial Destratification of Reservoirs," Technical Report E-79-1, US Army Engineer Waterways Experiment Station, Vicksburg, Miss.

Dortch, M. S., Fontane, D. G., and Wilhelms, S. C. 1976. "Dickey-Lincoln School Lakes Hydrothermal Model Study; Hydraulic Laboratory Investigation," Technical Report H-76-22, US Army Engineer Waterways Experiment Station, Vicksburg, Miss.

Fan, Luh-Nien, and Brooks, Norman H. 1969. "Numerical Solution of Turbulent Buoyant Jet Problems," Report No. KH-R-18, W. M. Keck Laboratory of Hydraulics and Water Resources, California Institute of Technology, Pasadena, Calif.

Fischer, Hugo, List, E. John, Koh, Robert C. Y., Imberger, Jorg, and Brooks, N. H. 1979. Mixing in Inland and Coastal Waters, Academic Press, New York.

Fontane, D. G., Dortch, M. S., Tate, C. H., Jr., and Loftis, B. 1977. "Marysville Lake Hydrothermal Study; Hydraulic and Mathematical Model Investigation," Technical Report H-77-5, US Army Engineer Waterways Experiment Station, Vicksburg, Miss.

Ford, D. E., Johnson, M. C., and Monusmith, S. G. 1980 (Jun). "Density Inflows to DeGray Lake, Arkansas," 2nd International Symposium on Stratified Flows, Trondheim, June 1980.

Holland, J. P., and Dortch, M. S. 1984. "Review of Guidance on Hydraulic Destratification," draft EWQOS Bulletin pending publication, US Army Engineer Waterways Experiment Station, Vicksburg, Miss.

Holland, J. P., Dortch, M. S., and Smith, D. R. 1982. "Norfork Lake, Arkansas, Temperature Analysis: Mathematical Model Investigation," Technical Report HL-82-12, US Army Engineer Waterways Experiment Station, Vicksburg, Miss.

Imberger, J., Thompson, R. T., and Fondry, C. 1976. "Selective Withdrawal from a Finite Rectangular Tank," Journal of Fluid Mechanics, Vol 78, Part 3, pp 489-512.

Kao, Timothy W. 1977. "Density Currents and Their Applications," Journal of the Hydraulics Division, ASCE, May 1977.

Koh, Robert C. Y. 1976. "Buoyancy-Driven Gravitational Spreading," Proceedings of the 15th International Coastal Engineering Conference, Honolulu, Hawaii, July 11-17, pp 2956-2975.

LeMéhauté, Bernard. 1976. An Introduction to Hydrodynamics and Water Waves, Springer Verlag.

Manins, P. C. 1976. "Intrusion into a Stratified Fluid," Journal of Fluid Mechanics, Vol 74, Part 3, pp 547-560.

Moretti, P. M., and McLaughlin, D. K. 1974. "Mixing Phenomena in Stratified Lakes," Report ER-75-ME-1, OWRR Project Number A-050-Oklahoma, The Oklahoma Water Resources Research Institute, Oklahoma State University. Stillwater, Okla.

Roberts, Philip J. W. 1982. "Mixing in Pumped-Storage Reservoirs," Proceedings of the Conference on Applying Research to Hydraulic Practice, Hydraulics Division of ASCE, August 17-20, 1982, Jackson, Miss.

BIBLIOGRAPHY

Bohan, J. P., and Gloriod, T. L. 1972. "Simultaneous, Multiple-Level Release From Stratified Reservoirs; Hydraulics Laboratory Investigation," Research Report H723, US Army Engineer Waterways Experiment Station, Vicksburg, Miss.

Bohan, J. P., and Grace, J. L., Jr. 1969. "Mechanics of Flow from Stratified Reservoirs in the Interest of Water Quality; Hydraulics Laboratory Investigation," Technical Report H-69-10, US Army Engineer Waterways Experiment Station, Vicksburg, Miss.

Bohan, J. P., and Grace, J. L., Jr. 1973. "Selective Withdrawal from Man-Made Lakes; Hydraulic Laboratory Investigation," Technical Report H-73-4, US Army Engineer Waterways Experiment Station, Vicksburg, Miss.

Dortch, M. S. 1976. "Effects of Flood Flows on Water Quality of Tioga-Hammond Lakes; Hydraulic Model Investigation," Technical Report H-76-11, US Army Engineer Waterways Experiment Station, Vicksburg, Miss.

Dortch, M. S. 1978. "Marysville Lake Hydrothermal Study; Hydraulic and Mathematical Model Investigation," Report 2, 2250-MW Project, US Army Engineer Waterways Experiment Station, Vicksburg, Miss.

Dortch, M. S. 1981. "Investigation of Release Temperatures for Kinzua Dam, Allegheny River, Pennsylvania; Hybrid Model Investigation," Technical Report HL-81-9, US Army Engineer Waterways Experiment Station, Vicksburg, Miss.

Dortch, M. S., Loftis, B., Fontane, D. G., and Wilhelms, S. C. 1976. "Dickey-Lincoln School Lakes Hydrothermal Model Study; Hydraulic Laboratory Investigation," Technical Report H-76-22, US Army Engineer Waterways Experiment Station, Vicksburg, Miss.

Fontane, D. G., and Bohan, J. P. 1974. "Richard B. Russell Lake Water Quality Investigation; Hydraulic Model Investigation," Technical Report H-74-14, US Army Engineer Waterways Experiment Station, Vicksburg, Miss.

Fontane, D. G., Dortch, M. S., Tate, C. H., Jr., and Loftis, B. 1977. "Marysville Lake Hydrothermal Study; Hydraulic and Mathematical Model Investigation," Technical Report H-77-5, US Army Engineer Waterways Experiment Station, Vicksburg, Miss.

George, J. F., Dortch, M. S., and Tate, C. H., Jr. 1980. "Selective Withdrawal Riser for Sutton Dam, West Virginia; Hydraulic Model Investigation," Technical Report HL-80-4, US Army Engineer Waterways Experiment Station, Vicksburg, Miss.

Gloriod, T. L., and Bohan, J. P. 1973. "Selective Withdrawal From Beech Fork Lake, Beech Fork River West Virginia; Hydraulic Model Investigation," Technical Report H-73-14, US Army Engineer Waterways Experiment Station, Vicksburg, Miss.

Loftis, B., Saunders, P. E., and Grace, J. L., Jr. 1976. "B. Everett Jordan Lake Water-Quality Study," Technical Report H-76-3, US Army Engineer Waterways Experiment Station, Vicksburg, Miss.

Smith, D. R., Holland, J. P., Loftis, B., and Tate, C. H., Jr. 1981. "Evaluation of In-Reservoir Cofferdam on Richard B. Russell Reservoir and Hydropower Releases; Hybrid Model Investigation," Technical Report HL-81-12, US Army Engineer Waterways Experiment Station, Vicksburg, Miss.

Wilhelms, S. C. 1976. "Bay Springs Lake Water-Quality Study; Hydraulic Laboratory Investigation," Technical Report H-76-7, US Army Engineer Waterways Experiment Station, Vicksburg, Miss.

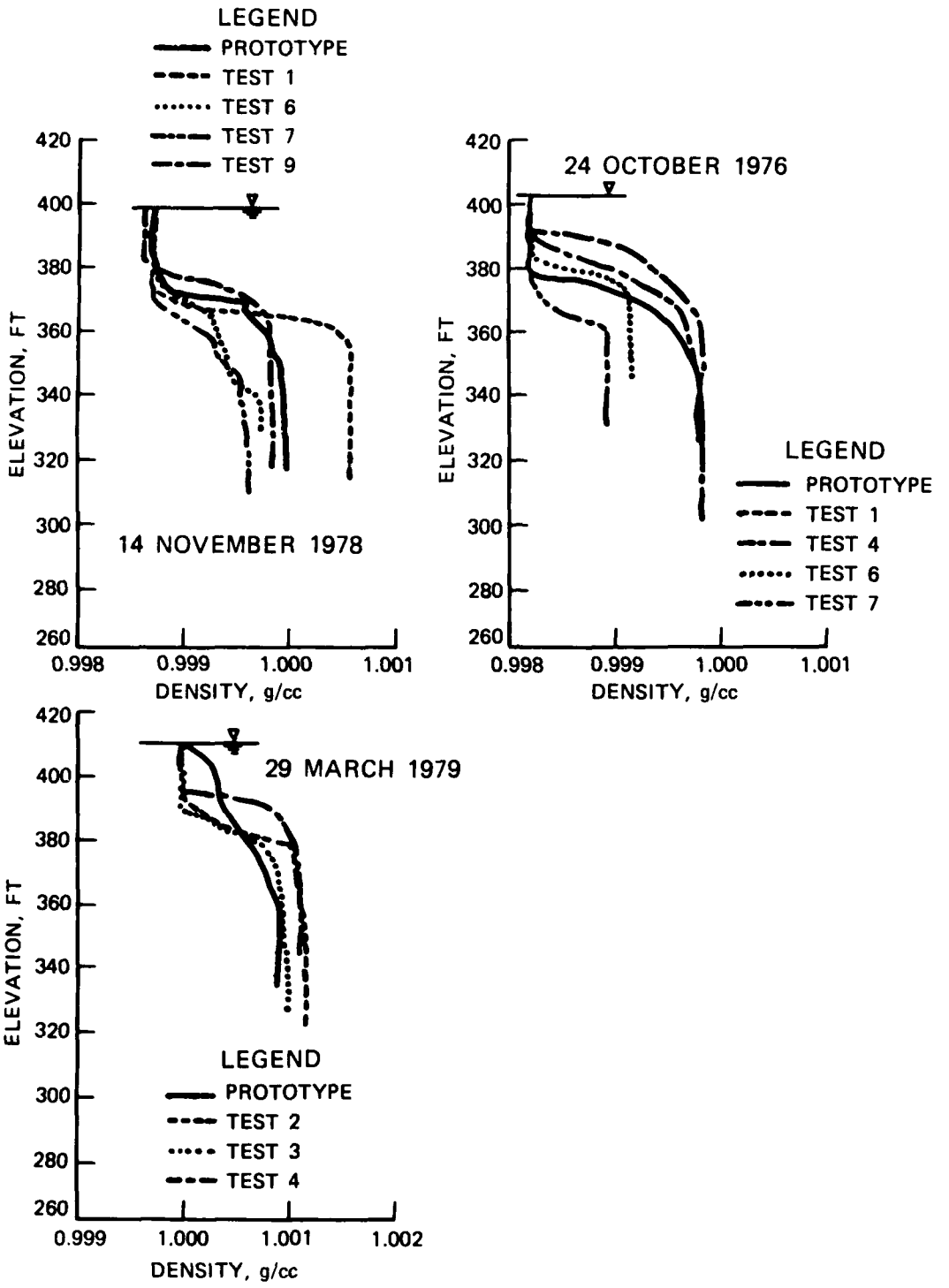

PROTOTYPE AND MODEL STRATIFICATION FOR DEGRAY LAKE FLOOD EVENTS

PLATE 1

PLATE 2

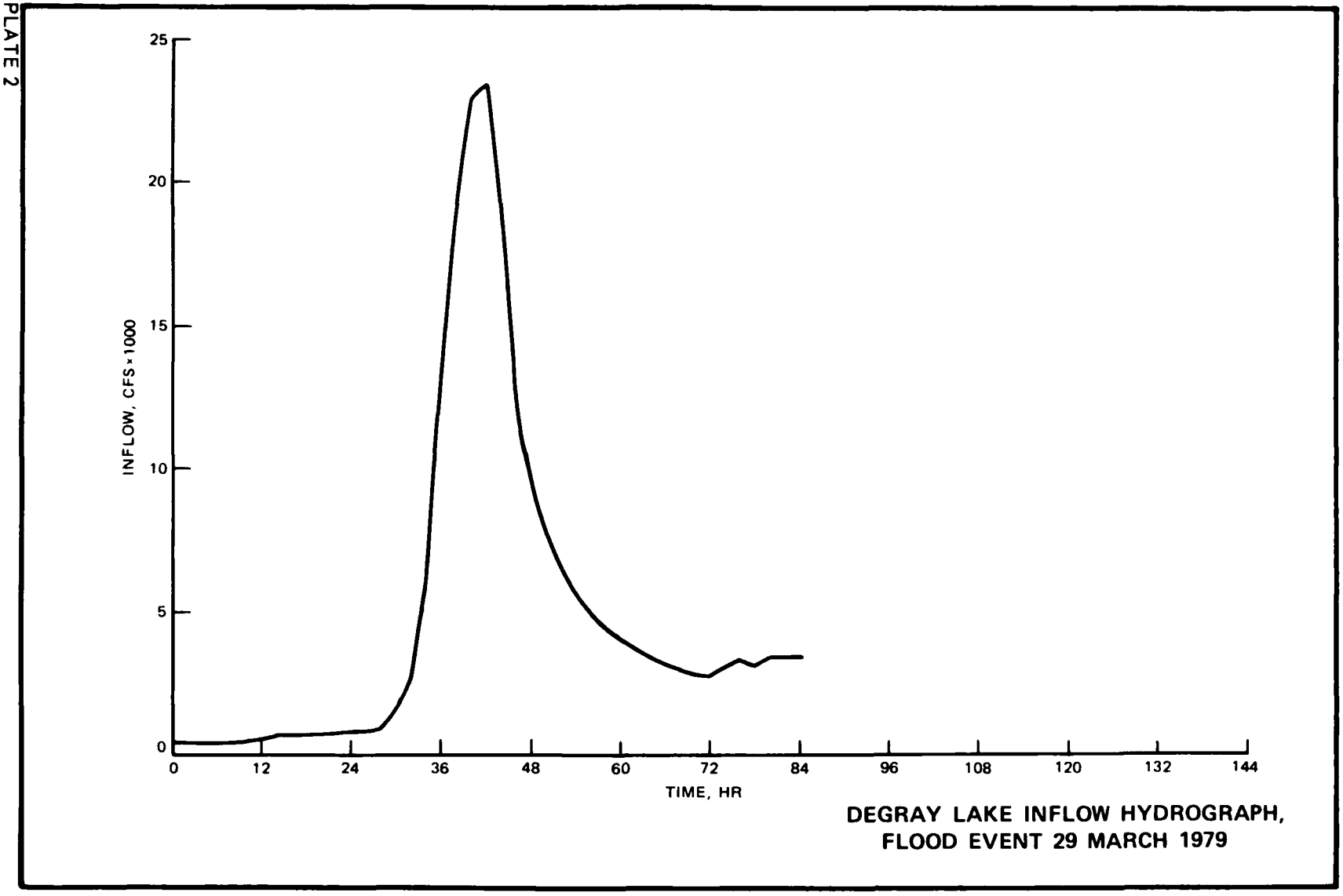

DEGRAY LAKE INFLOW HYDROGRAPH,
FLOOD EVENT 29 MARCH 1979

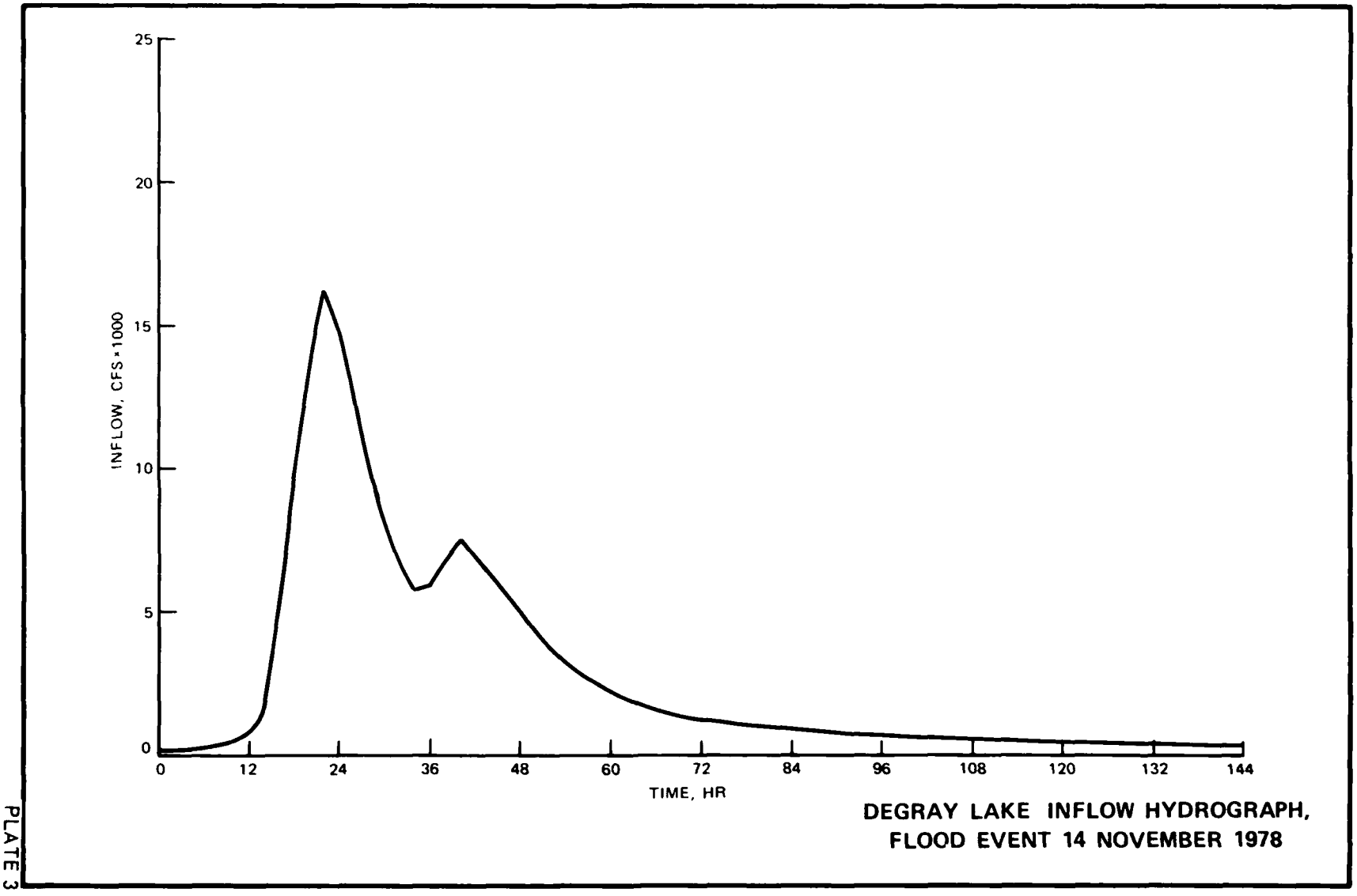

DEGRAY LAKE INFLOW HYDROGRAPH,
FLOOD EVENT 14 NOVEMBER 1978

PLATE 3

PLATE 4

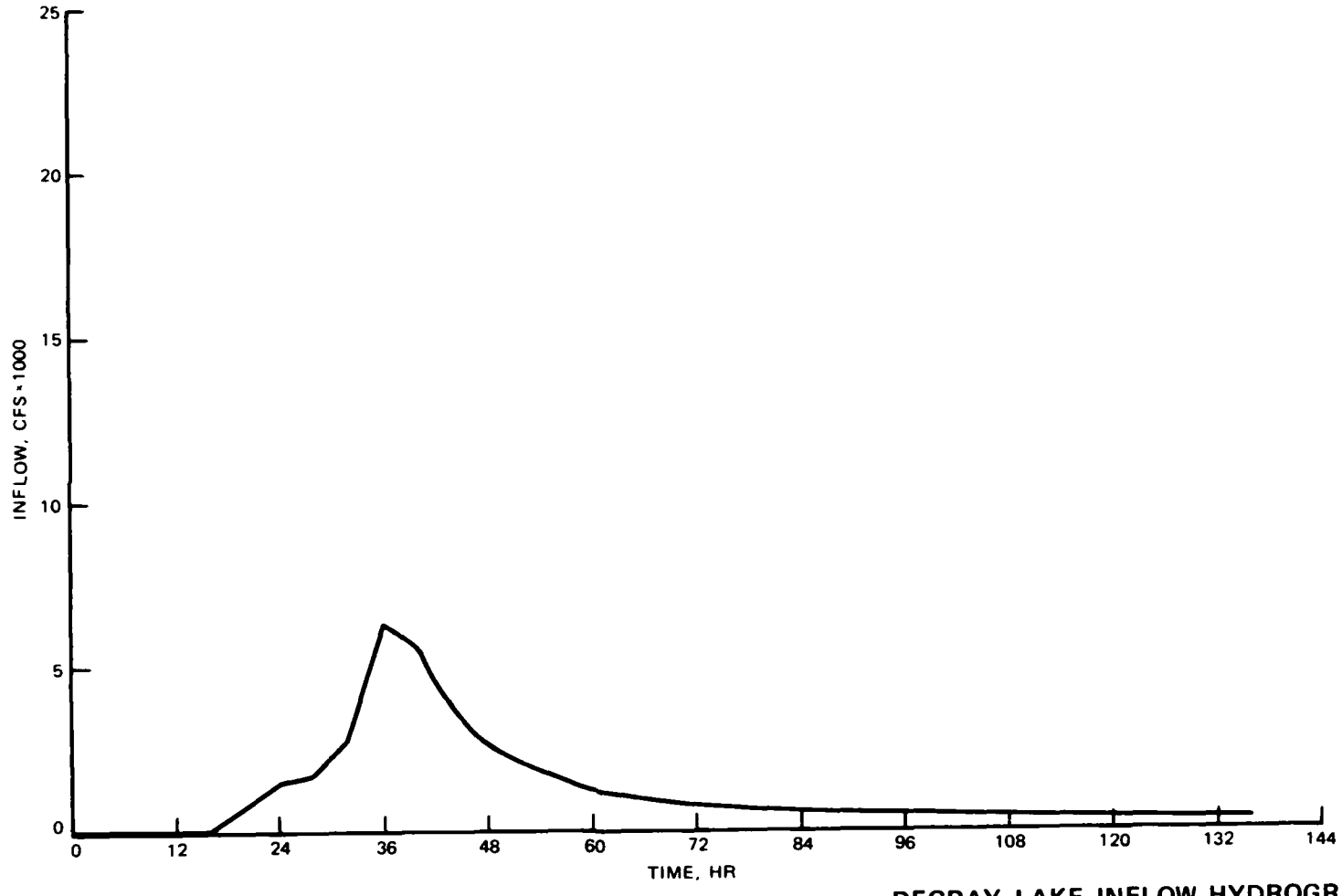

DEGRAY LAKE INFLOW HYDROGRAPH,
FLOOD EVENT 24 OCTOBER 1976

APPENDIX A: MECHANICS OF INTERFLOW AND OVERFLOW DENSITY CURRENTS

Interflow

1. In his work on interflows (intrusions), Manins (1976)* introduced a neutrally buoyant inflow (evenly distributed laterally) at the mid-depth of a linearly stratified laboratory tank (Figure A1). His experiments were in the nonviscous range where there is a balance of pressure and inertia forces. In this range, the observed intrusion length ℓ was linearly proportional to time t. Thus, the nose velocity or intrusion speed c was constant for a given set of conditions. Through dimensional analysis, the intrusion speed reduced to

$$c \propto (qN)^{1/2}$$

where

q = volumetric inflow rate per unit width

N = buoyancy frequency, $\sqrt{\frac{-g}{\rho_o}\frac{d\rho}{dz}}$

ρ_o = inflow density and density of ambient fluid at mid-depth

z = length in vertical direction

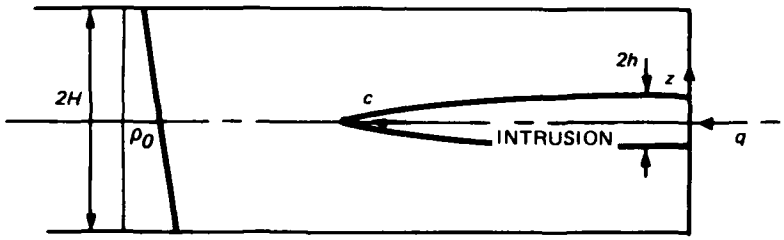

Figure A1. Sketch of intrusion into a stratified fluid (Manins 1976)

Manins' experimental data and analytical results indicated that the constant of proportionality in the above relationship was about 0.85. The intrusion thickness near the source was also constant during each test, although the thickness does taper toward the nose of an intrusion.

---

* See References at the end of the main text.

Dimensional analysis yielded for the half thickness

$$h \propto \left(\frac{q}{N}\right)^{1/2}$$

Manins' data indicated that h varied nonlinearly with $(q/N)^{1/2}$. This was not the case for c versus $(qN)^{1/2}$. For Manins' thickness data, $h/[(q/N)^{1/2}]$ varied between about 1.7 and 1.0, where h is half the intrusion thickness near the source.

2. Manins analytically showed that there are unsteady flow regions due to columnar wave disturbances which are able to propagate upstream faster than the relative flow velocity c. There are M such wave fronts defined by

$$M = \text{integer part} \left(\frac{NH}{\pi c}\right)$$

where H is half the channel depth. The number of wave fronts tend to affect the intrusion speed and thickness. The larger N is, the larger M is. As M increases (for different conditions) the internal Froude number of the intrusion decreases. Manins' experimental data supported this result as shown in Figure A2 where the internal Froude number F_r defined by

$$F_r = \frac{c}{Nh}$$

is plotted against M. The curves are upper and lower bounds from an analytical flow model. If the flow is completely steady throughout without the columnar disturbances, and the disturbance of the ambient density gradient above and below the instrusion is negligible, the F_r would be unity; but as M increases, F_r decreases from unity. For Manins' experimental results, F_r varied from about 1.0 to 0.40. Noting F_r is dependent upon c and h, it is evident c and h are influenced by columnar waves. Manins concluded that h was more strongly influenced by columnar waves than c as h was not linearly related to $(q/N)^{1/2}$ (paragraph 1 of this appendix). Thus, although the intrusion speed and thickness are steady in the nonviscous regime, internal waves affect the intrusion speed and thickness (primarily the thickness) with

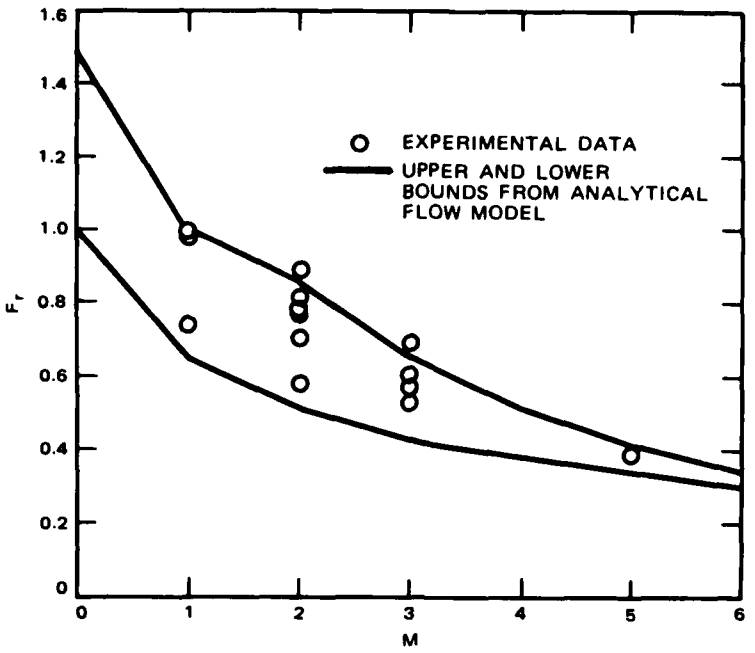

Figure A2. Internal Froude number as a function of the number of forward propagating columnar modes (Manins 1976)

the net effect of reducing F_r for higher M. Manins did not give any criteria for when the intrusion is in the viscous or nonviscous regime.

3. Manins' results were for a linear stratification. A two-layer stratification with an inflow at the interface is shown in Figure A3.

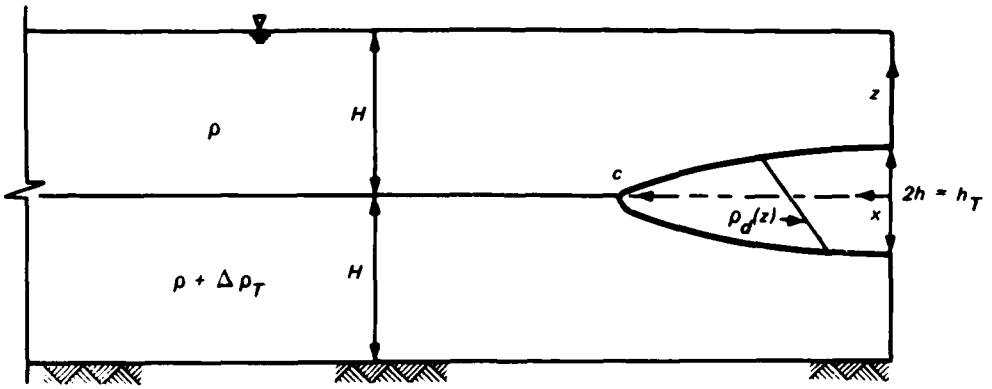

Figure A3. Two-layer stratification

Following from Kao (1977) the intrusion speed c of this type of interflow condition can be described for the portion above the interface by

$$c = \left(2 \frac{\Delta\rho}{\rho} gh - \beta g h^2\right)^{1/2} \qquad \text{(A1)}$$

where

$\Delta\rho = \rho_d(z) - \rho$

$\rho_d(z)$ = density gradient within the density current

ρ = density of upper layer

h = vertical distance from elevation of neutral buoyancy to upper limit of interflow

$$\beta = \frac{-1}{\rho} \frac{d\rho_d(z)}{dz}$$

Assuming that the density gradient within the density current is linear, Equation A1 reduces to

$$\frac{c}{\sqrt{\frac{\Delta\rho}{\rho} gh}} = 1.0 \qquad \text{(A2a)}$$

Therefore, for the two-layer stratification, the F_r of the intrusion is approximately unity. If the thickness of the density current is symmetrical about the interface,

$$\Delta\rho = \frac{\Delta\rho_T}{2}$$

$$h = \frac{h_T}{2}$$

where

$\Delta\rho_T$ = the total density differences of the two-layer stratification

h_T = the total thickness of the intrusion

Equation A2a can be written as

$$\frac{c}{\sqrt{\frac{\Delta\rho_T}{\rho} gh_T}} = 0.50 \qquad \text{(A2b)}$$

4. The stratification of reservoirs is characteristic of the two-layer stratification in the sense that there exists a well-mixed epilimnion and hypolimnion. These two layers are joined by a metalimnion that has a continuous, often linear, stratification. This type of stratification complicates any method for determining M, F_r, c, and h. As a first approximation, one can assume that reservoir stratification is more characteristic of two layers, ignore the effect of internal waves, and assume the F_r of the intrusion is unity. Thus, for lake stratification, Equation A2 would be used to compute c if h_T is known. Figure A4 demonstrates how the variables of Equation A2 would be applied to a thermocline-type stratification.

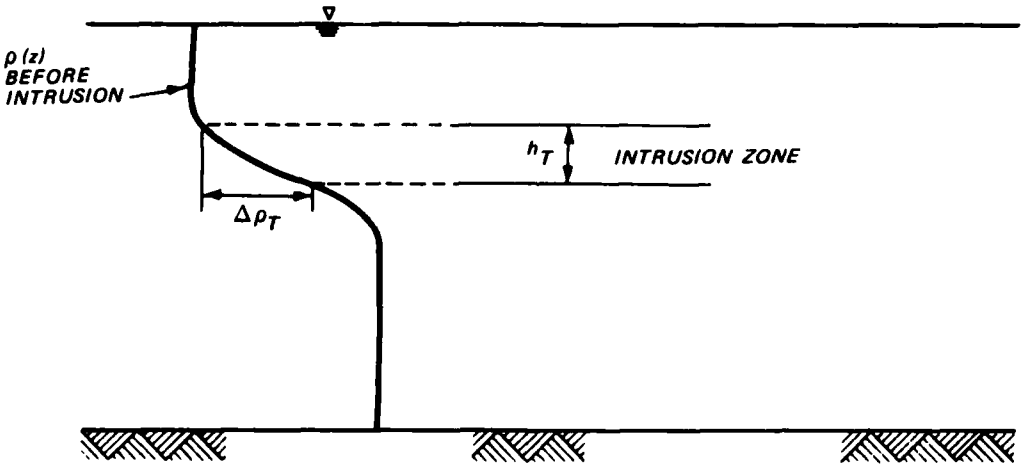

Figure A4. Definition sketch for thermocline-type stratification

5. Assuming that Equation A2b can be used to estimate intrusion speed, one must first know h_T to use the equation. The thickness of the intrusion is nonuniform and decreases from h_T near the upstream source to zero at the tip of the nose. With q constant, the average flow velocity increases as thickness decreases with the maximum velocity c existing at the nose. Since the flow is nonuniform, the use of

$q = ch_T$ is not the appropriate relationship to couple with Equation A2 to solve for c and h_T. However, it is true that q is proportional to ch_T and, thus, after rearranging and making use of Equation A2,

$$h_T \propto \left(\frac{q}{\sqrt{\frac{\Delta\rho_T}{\rho} g}} \right)^{2/3} \tag{A3}$$

Relationship A3 can also be obtained from $h_T \propto (q/N)^{1/2}$ (paragraph 1) by approximating N as $\sqrt{g/\rho(\Delta\rho_T/h_T)}$. A study of Manins' data indicated that the proportionality constant for relationship A3 varied between $2.5 \left\{ h/\left[(q/N)^{1/2}\right] = 1.0 \right\}$ and about $5.1 \left\{ h/\left[(q/N)^{1/2}\right] = 1.7 \right\}$ with the variability due to variations in M (paragraphs 1 and 2). Using approximately the mean value of Manins' data for the thickness relationship results in

$$h_T = 3.0 \left(\frac{q}{\sqrt{\frac{\Delta\rho_T}{\rho} g}} \right)^{2/3} \tag{A4}$$

for a symmetrical interflow. With $\Delta\rho_T$ dependent upon h_T, h_T can be estimated from an iterative solution of Equation A4. With a value for h_T, c can be estimated (for reservoir stratification) from Equation A2. The reservoir width used for computing q (for Equation A4) would be taken near the station at which the inflow separates from the bottom and becomes an interflow.

6. The results of Manins can be used for an intrusion that is asymmetric about the neutrally buoyant layer as follows:

$$h_{1,2} = 1.2 \left(\frac{q}{\sqrt{\frac{\Delta\rho_{1,2}}{\rho} g}} \right)^{2/3} \tag{A5}$$

where

$h_{1,2}$ = the intrusion thickness below (1) and above (2) the neutrally buoyant layer

$\Delta\rho_{1,2}$ = the density difference between the elevation of lower limit (1) or upper limit (2) of the intrusion thickness and the elevation of the neutrally buoyant layer

It should be emphasized that for the thermocline-type stratification the F_r will be less than 1.0 and therefore the use of Equation A2 for interflow speed will provide only an estimate. If a linear stratification was observed, Manins' results could be used to obtain a more accurate estimate. For the linear case, $c = 0.85(qN)^{1/2}$, where N is known and h is not required to find c. After calculating c, the values for M, F_r, and h_T can be determined (paragraph 2). But for the arbitrary thermocline-type stratification, N is not known, and c, M, F_r, and h cannot be calculated directly from Manins' results; thus, the approximations above are proposed. It must also be emphasized that the above discussions pertain only to two-dimensional intrusions.

7. Imberger, Thompson, and Fondry (1976) suggest that an interflow intrusion is in the nonviscous range when

$$t \leq \frac{q}{N\nu}$$

where t is the elapsed time from when the intrusion began. Thus $\ell = ct$ is the intrusion length. Solving Equation A4 for q, using $t = \ell/c$ and $N = \sqrt{(\Delta\rho_T/h_T)(g/\rho)}$ and substituting Equation A2b for c, Imberger's relation can be rewritten as

$$\frac{h_T^{5/2}\sqrt{\frac{\Delta\rho_T}{\rho}\,g}}{\nu\ell} \geq 10.4 \qquad \text{(A6)}$$

In this form Equation A6 represents the product of a hydraulic grade line h_T/ℓ and the densimetric Froude-Reynolds number $\left[h_T^{3/2}\sqrt{(\Delta\rho_T/\rho)g}/\nu\right]$. Equation A6 provides criteria for cases where a nonviscous interflow exists.

Overflow

8. Koh (1976) summarizes the results for a variety of buoyancy-driven gravitational surface flows. His results for the two-dimensional continuous surface inflow pertain mostly to reservoir overflow density currents. For this case, Koh presented analytical and experimental results that compared closely and related the speed of advance, for intermediate travel times (nonviscous regime), as

$$c = 0.8 \left(\frac{6}{\pi} \frac{\Delta\rho}{\rho} gq \right)^{1/3}$$

where $\Delta\rho$ is now the density difference of the inflowing water and the receiving water. The above equation reduces to

$$c = \left(\frac{\Delta\rho}{\rho} gq \right)^{1/3} \tag{A7}$$

9. From Koh's (1976) results it was concluded for a surface current that

$$h_K = 1.24 \left(\frac{q}{\sqrt{\frac{\Delta\rho}{\rho} g}} \right)^{2/3} \tag{A8}$$

where h_K is the thickness of the overflow density current. Equation A8 is fairly consistent with Equation A5, the upper or lower thickness equation for an interflow. If Equation A8 is solved for q and substituted for q in Equation A7, Equation A7 can be rewritten

$$c = 0.90 \sqrt{\frac{\Delta\rho}{\rho} gh_K}$$

which is close to the previous interflow result of F_r near unity (paragraphs 2 and 3).

10. It was observed from Koh's (1976) results that the surface intrusion length was linearly proportional (nonviscous regime) to time for t/t_o less than approximately 0.5 to 1.0. For t/t_o greater

than this range, the intrusion length was proportional to $t^{4/5}$ (viscous regime). Thus, the criterion for a nonviscous overflow is

$$\frac{t}{t_o} \leq 0.5 \text{ to } 1.0$$

where the parameter t_o is defined as

$$t_o = \frac{16q^2}{3\pi^2\nu} \left(\frac{\pi}{6 \frac{\Delta\rho}{\rho} gq} \right)^{2/3}$$

Substitution of this relation for t_o into the previous relationship, and using $t = \ell/c$ with Equation A7 for c and Equation A8 for q results in

$$\frac{h_K^{5/2} \sqrt{\frac{\Delta\rho}{\rho} g}}{\ell\nu} \geq 4.88 \text{ to } 9.75 \qquad \text{(A9)}$$

The larger value for the right side of Equation A9 is very close to the value in Equation A6. A range of values for the right side of Equation A9 is presented because the data reported by Koh (1976) gradually transition from the nonviscous to the viscous regime.

11. To summarize, the following equations may be used for estimating interflow and overflow conditions:

Interflows	Equation
Nonviscous range	A6
Thickness	A4 and A5
Speed	A2

Overflows	Equation
Nonviscous range	A9
Thickness	A8
Speed	A7

In the nonviscous regime, the thickness near the source and the speed of the intrusion are constant. In the viscous range, the intrusion speed

decreases with time and the thickness increases with time. The viscous regime will not be discussed in any greater detail because it is not practical, and most difficult, to physically model with Froudian scaling criteria (see Part III of the main text).

APPENDIX B: PROCEDURE FOR SIZING A ROUND BUOYANT JET IN A DISTORTED MODEL

1. If the entrainment (dilution) of a buoyant jet is known, it is possible to size the jet in the distorted-scale physical model to give the same dilution. A round buoyant jet discharging horizontally into a linearly stratified reservoir has an ultimate (finite) dilution that depends upon the specific physical conditions. Roberts (1982)* reported procedures for determining the dilution for this type of jet. He expanded upon the results of Fan and Brooks (1969) to include the conditions of a weakly buoyant jet. These results, which include weakly and strongly buoyant jets, are discussed and the procedure for properly sizing (scaling) a round jet is presented in subsequent paragraphs.

2. Consider the following known parameters for a prototype jet: the initial (source) volume flux of the jet before entrainment Q, and the area of efflux A, the difference in density between the jet and ambient $\Delta\rho_o$, and the stratification parameter ε. Mathematically expressed

$$\Delta\rho_o = \rho - \rho_o$$

$$\varepsilon = -g/\rho \; d\rho/dz$$

where

ρ_o = initial density of jet

ρ = ambient density at the level of jet efflux

g = acceleration due to gravity

$d\rho/dz$ = slope of ambient density gradient at level of efflux

With these prototype values, it is possible to calculate the exit velocity u_o, momentum flux M, and buoyancy flux B as follows:

$$u_o = \frac{Q}{A}$$

$$M = Qu_o$$

$$B = \frac{g\Delta\rho_o}{\rho} Q$$

---

* See References at the end of the main text.

3. By combining ε, Q, M, and B, characteristic lengths can be formed that describe jet properties. The most convenient are:

$$\ell_Q = \frac{Q}{M^{1/2}} = \sqrt{A}$$

$$\ell_M = \frac{M^{3/4}}{B^{1/2}}$$

$$\ell_\varepsilon = \left(\frac{M}{\varepsilon}\right)^{1/4}$$

where ℓ_Q is proportional to the distance over which the nozzle geometry is important in determining the jet properties; ℓ_M is proportional to the distance over which the initial momentum flux is important relative to the initial buoyancy flux; and ℓ_ε is proportional to the distance over which the source momentum flux is important relative to the stratification. Jet properties and characteristics can be expressed as ratios of these lengths.

4. Through dimensional analysis, total volume flux μ in the jet following entrainment can be related to ℓ_Q/ℓ_ε and ℓ_M/ℓ_ε in the form

$$\frac{\mu\varepsilon^{1/4}}{M^{3/4}} = f\left[\frac{\ell_Q}{\ell_\varepsilon}, \frac{\ell_M}{\ell_\varepsilon}\right] \qquad \text{(B1)}$$

The dimensionless parameters of Equation B1 are plotted in Figure B1 for the case of a round buoyant jet discharging horizontally into a linearly stratified ambient as reported by Roberts (1982).

5. From Figure B1 it is possible to determine μ for the prototype jet, and the entrainment parameter E which is related to μ by

$$E = \frac{\mu - Q}{Q} = \frac{\text{entrained volume flux}}{\text{initial volume flux}}$$

Mean dilution of the jet is defined as μ/Q. To preserve the dilution of the prototype jet in the model requires

$$\frac{\mu_R}{Q_R} = 1.0 \qquad \text{(B2)}$$

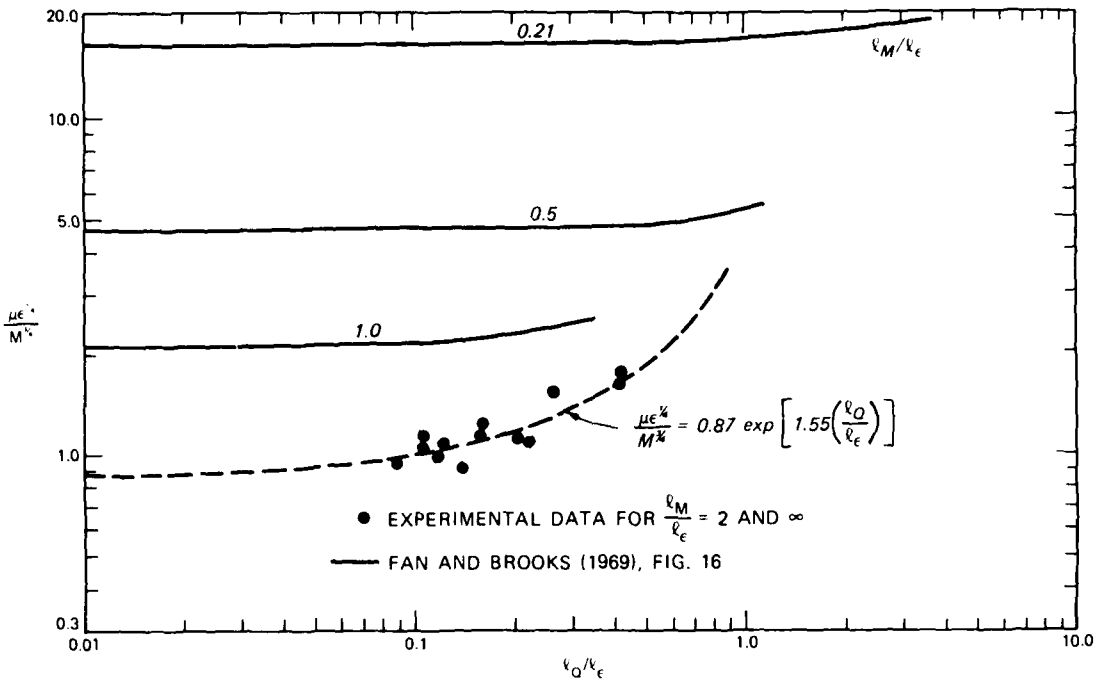

Figure B1. Dimensionless volume flux parameter for round buoyant jets discharging horizontally into a linearly stratified ambient

or

$$E_R = 1.0$$

where R represents the prototype-to-model ratio of the parameter. With μ_p (p = prototype), μ_m (m = model) can be calculated from Equation B2. Since the discharge ratio Q_R is scaled according to Froudian criteria $Q_R = X_R Y_R^{3/2}$. Therefore,

$$\mu_m = \frac{\mu_p}{Q_R} = \frac{\mu_p}{X_R Y_R^{3/2}} \qquad \text{(B3)}$$

where X_R, Y_R = prototype-to-model ratio for length in horizontal and vertical directions, respectively. If the water density differences of the model stratification are equal to that of the prototype, then the stratification parameter is scaled as

$$\varepsilon_m = \frac{-gd\rho_m}{\rho_m dz_m} = \frac{-gd\rho_p}{\rho_p dz_m} = \varepsilon_p Y_R \tag{B4}$$

The momentum flux for the model can then be written

$$M_m = Q_m u_{o_m} = \frac{Q_m^2}{A_m} = \frac{Q_p^2 A_R}{Q_R^2 A_p} = \frac{M_p A_p}{\left(X_R Y_R^{3/2}\right)^2} \tag{B5}$$

where A_R = area scale ratio in a vertical plane. Combining Equations B3 through B5

$$\left(\frac{\mu\varepsilon^{1/4}}{M^{3/4}}\right)_m = \left(\frac{\mu\varepsilon^{1/4}}{M^{3/4}}\right)_p \frac{X_R^{1/2} Y_R}{D_R^{3/2}} \tag{B6}$$

where D_R is the prototype-to-model ratio of the jet source diameter. The parameter $\left[(\mu\varepsilon^{1/4})/(M^{3/4})\right]_p$ was determined previously from Figure B1. Equation B6 has two unknowns $\left[(\mu\varepsilon^{1/4})/(M^{3/4})\right]_m$ and D_R.

6. The jet characteristic length ratios of paragraph 3 of this appendix can be expanded to the form

$$\frac{\ell_Q}{\ell_\varepsilon} = \frac{A^{3/4} \varepsilon^{1/4}}{Q^{1/2}}$$

$$\frac{\ell_M}{\ell_\varepsilon} = \frac{Q^{1/2}}{\sqrt{\frac{g\Delta\rho_o}{\rho}} A^{1/2} \varepsilon^{1/4}}$$

From the above relations with $\Delta\rho_R = 1.0$, the following relationships result

$$\left(\frac{\ell_Q}{\ell_\varepsilon}\right)_m = \left(\frac{\ell_Q}{\ell_\varepsilon}\right)_p \frac{X_R^{1/2} Y_R}{D_R^{3/2}} \tag{B7}$$

$$\left(\frac{\ell_M}{\ell_\varepsilon}\right)_m = \left(\frac{\ell_M}{\ell_\varepsilon}\right)_p \frac{D_R}{X_R^{1/2} Y_R} \qquad \text{(B8)}$$

In Equations B6, B7, and B8, the unknowns are $\left(\mu\varepsilon^{1/4}/M^{3/4}\right)_m$, $\left(\ell_M/\ell_\varepsilon\right)_m$, $\left(\ell_Q/\ell_\varepsilon\right)_m$, and D_R. A trial-and-error solution procedure is therefore necessary to solve for D_R, the scale ratio needed to size the model jet diameter.

7. By assuming a value for D_R, Equation B6 may be solved for $\left(\mu\varepsilon^{1/4}/M^{3/4}\right)_m$; Equations B7 and B8 may be solved for $\left(\ell_Q/\ell_e\right)_m$ and $\left(\ell_M/\ell_\varepsilon\right)_m$, respectively. Using these two-length ratios and Figure B1, a value for $\left(\mu\varepsilon^{1/4}/M^{3/4}\right)_m$ can be determined. This value is compared to that calculated from Equation B6. A new value for D_R would be assumed and the procedure repeated until the value for $\left(\mu\varepsilon^{1/4}/M^{3/4}\right)_m$ determined from Figure B1 agrees with that calculated with Equation B6. The final value for D_R can be used to determine the required source diameter of the model jet. The model jet should be checked to ensure that turbulent flow will exist. If turbulent flow cannot be ensured, it may be necessary to reduce the model scale ratios X_R and/or Y_R

END

DTIC

4-86